ARMY RESEARCH LABORATORY

Feasibility of Magnetic Particle Films for Curie Temperature-Controlled Processing of Composite Materials

by Eric D. Wetzel and Bruce K. Fink

ARL-TR-2431 March 2001

The findings in this report are not to be construed as an official Department of the Army position unless so designated by other authorized documents.

Citation of manufacturer's or trade names does not constitute an official endorsement or approval of the use thereof.

Destroy this report when it is no longer needed. Do not return it to the originator.

Army Research Laboratory
Aberdeen Proving Ground, MD 21005-5066

ARL-TR-2431 **March 2001**

Feasibility of Magnetic Particle Films for Curie Temperature-Controlled Processing of Composite Materials

Eric D. Wetzel and Bruce K. Fink
Weapons and Materials Research Directorate, ARL

Abstract

The feasibility of using magnetic particulate susceptor materials for induction heating during bonding of polymer matrix composite materials is investigated. If properly designed, these systems should rapidly heat to the particulate material Curie temperature and dwell at that temperature without feedback control. This performance is only possible by maximizing hysteresis heating while eliminating eddy current heating and shielding effects. Models of eddy current heating, hysteresis heating, field penetration thickness, and heat transfer in a particulate film are presented. These models are then used to predict heating behavior of particulate films containing metallic ferromagnetic (nickel), hard magnetic (strontium ferrite), and soft magnetic (nickel zinc ferrite) materials. The results show that soft or semi-hard insulating magnetic materials are best suited for susceptor particles for a broad range of potential military applications. Polymer films with around 10% volume fraction of these materials should be capable of heating rates up to 100 °C/s in moderate strength 1–10 MHz induction fields.

Table of Contents

List of Figures

List of Tables

INTENTIONALLY LEFT BLANK.

1. Introduction

1.1 Joining and Repair of Composite Materials. The goal of creating a light-weight, rapid-insertion, highly lethal, yet survivable ground force for the Army of 2010 and beyond has led to an increased emphasis on using fiber-reinforced polymer matrix composite materials for both structural and armor components. A major hurdle towards implementation of these materials, however, is developing mature technologies for joining and repair of composite materials.

In order to incorporate composite components into large assemblies, they must be joined to many different materials, including metals, ceramics, and other polymeric composites. The simplest joining method is mechanical fasteners [1]. However this approach results in poor load transfer, stress concentrations, high parts count, and increased weight. For these reasons, most composites are joined using surface bonding techniques such as adhesives or thermoplastic fusion bonding. Adhesives often provide adequate bond strength and allow bonding between dissimilar materials, but typically require long process times and extensive surface preparations [2]. Recent work has shown that adhesive cure times can be shortened without bond strength reduction through the use of elevated temperature cure cycles [3]. Thermoplastic fusion bonding joins materials through the heating, melting, and consolidation of a thermoplastic interface [4, 5]. Thermoplastic composites can be directly joined to other thermoplastics, metals, or ceramics using this technique. Incorporating a fusible thermoplastic surface layer onto thermoset composites, such as through the diffusion enhanced adhesive (DEA) technique [6], also allows application of thermoplastic fusion bonding to thermoset composites. As compared with conventional adhesives, fusion bonding typically offers shorter process times and little or no surface preparation.

For both accelerated-cure adhesives and fusion bonding, localized heating is required at the bondline. The amount of heat generated must be sufficient to raise the interface to 100° - 200°C for adhesives, and 150°-400°C for fusion bonding of engineering thermoplastics. Higher heating power allows for faster heating rates, reducing process times and localizing thermal effects to the interface. Localized heating at the interface is critical to successful bonding in order to minimize energy requirements and prevent thermal degradation of the surrounding material [7]. Direct interface heating also allows the joining of thick parts, which are difficult to heat using through-thickness heating methods.

A number of interface heating techniques have been developed, including ultrasonic welding [8], spin welding [9], and resistive heating [4, 5]. In ultrasonic welding, the two materials to be joined are held in contact and vibrated at high frequencies, generating frictional heat

at their interface. This technique is best suited to small parts and simple geometries. Spin welding works on similar principles, except that frictional heating is generated by relative rotational motion between the two components. Both spin and ultrasonic welding are forms of thermoplastic fusion bonding, and are not applicable to accelerated-cure adhesives. In resistive heating, electrical current is passed through an interface implant made of metal screen or continuous carbon fibers, which rapidly heats due to Joule heating. This approach has shown great promise for joining composites through both fusion bonding and elevated-temperature adhesives, with rapid heating rates, and high control and repeatability. However, there are a number of limitations to this method. The need to establish direct electrical contact with the implant places geometric limitations on its applicability. Power and implant resistance limitations require large joints to be made in many small steps. The need for direct application of high electrical currents raises safety concerns for field applications. And the presence of the resistive implant at the interface often weakens the final bond strength.

1.2 Induction Heating. Induction heating has been proposed as a means of interface heating polymer matrix composite materials [10–13]. In this approach, a susceptor material is placed at the bondline and exposed to an alternating magnetic field. The magnetic field can induce heating in the susceptor material through two mechanisms. If the susceptor material is conductive, currents are induced in the susceptor, which then heats due to resistive effects. This mode of heating is called eddy current heating, and is the only source of heating in nonmagnetic susceptor materials such as stainless steel and carbon fibers. If the susceptor is magnetic, hysteresis losses associated with the magnetization-demagnetization cycle causes additional heating. This mode of heating is called hysteresis heating.

A major advantage of the induction method is that it is a noncontact technique. Typically the induction head, which generates the magnetic field, is placed on the surface of the parts to be joined. The magnetic field penetrates to the interface where it causes the susceptor material to heat. Since direct access to the interface is not needed, induction heating offers great geometric flexibility, applicability to large bond areas, and improved safety as compared with resistive heating methods.

A further benefit of the induction joining technique, when implemented with thermoplastic fusion bonding, is that it could improve the repairability of composite structures in the field. Because the susceptor material remains embedded at the interface, at any time the interface can be reheated through application of a magnetic field. A joint which becomes damaged at the bondline can be rejoined by remelting and reconsolidating the interface, potentially recovering the original bond strength. Components which are damaged away from the bondline can

be repaired by remelting the interface, removing the damaged component, and rebonding a replacement component.

1.3 Particulate Susceptor Materials. Traditional induction susceptor materials include metal screens and carbon fiber implants. However, a novel approach which offers many advantages over traditional susceptor materials is to disperse magnetic microparticles at the interface [14]. The small size of the particles reduces the mechanical degradation of bond strength associated with traditional macroscopic susceptor materials. Particulate susceptors also offer unique geometric possibilities, such as flowable and moldable susceptor materials.

The principal advantage of particulate susceptor materials, however, is their unique heating behavior. If the particle is small enough or resistive enough, there is insufficient current path for appreciable resistive heating. In this situation all of the heating is due to hysteresis effects. A special property of magnetic materials is the presence of a Curie temperature, which marks the transition of the material from a ferromagnetic or ferrimagnetic state to a paramagnetic state. A material which is above its Curie temperature loses its magnetic properties, and can no longer generate hysteresis heating. Therefore, if magnetic particulate susceptors can be designed which possess a Curie temperature and do not heat due to eddy current effects, they cannot be heated inductively above their Curie temperature.

This property allows the creation of specialized susceptors which "automatically" maintain a desired processing temperature without the need for external control. As compared with traditional induction bonding techniques, this feature greatly improves process control while reducing the necessary equipment sophistication and operator expertise. This method also provides an opportunity for multi-material cures. By layering different materials with specific microparticle compositions at each interface, a single imposed magnetic field can be used to simultaneously heat two interfaces to different dwell temperatures. A thermoplastic fusion bonding technique utilizing induction heating of magnetic microparticles therefore possesses tremendous potential as a simple, flexible, noncontact, highly controllable joining process for composite materials.

1.4 Objectives and Approach. In this report we evaluate the feasibility of using particulate susceptor materials for induction bonding and repair of composite materials. In addition, we will provide guidance as to what materials and equipment are best suited for this application, and which research thrusts are most crucial towards implementation and sophistication of this technique. The performance and design goals for this application are:

- Ensure automatic temperature control by choosing a system with high hysteresis heating and low eddy current heating.
- Enable application to elevated temperature adhesives, which require processing temperatures from $\sim 100°to200°$C, and all engineering thermoplastics, which require processing temperatures from $\sim 150°to400°$C.
- Keep equipment power, size, and cost within reasonable bounds for widespread field implementation.

Because our objective is only to provide general recommendations on particulate induction heating, all calculations are performed to order-of-magnitude accuracy. This level of accuracy is sufficient to eliminate unreasonable approaches, compare vastly different approaches, and estimate feasibility. The creation of quantitatively accurate models for design and control of specific induction processes will be presented in future reports.

There has been considerable research on the microscopic mechanisms which cause hysteresis in magnetic materials, most notably domain wall motion [15–19] and magnetization rotation [20–22]. However, these studies have yet to provide a reliable means of quantitatively predicting macroscopic magnetic properties and behaviors from first principles. Therefore, we will only address microscopic processes in order to get a qualitative understanding of some macroscopic behavior. The analytical modeling of heating processes will instead be based on reported macroscopic magnetic properties.

This report is organized as follows. In section 2, mathematical models of the relevant process physics are derived. In section 3, these process models are used to determine the design parameters for this application. In section 4, three specific material systems, representing three distinct classes of magnetic materials, are evaluated based on the design parameters. Sections 5 and 6 discuss and summarize the results of this report, and section 7 proposes future directions for development of this technology.

2. Process Physics Models

In this section we construct mathematical models of the relevant electromagnetic and heat transfer phenomenon which are involved in the proposed induction heating approach.

2.1 Magnetic Theory Preliminaries and Definitions. When a magnetic material is placed in a magnetic field, the magnetic field is locally augmented through atomistic

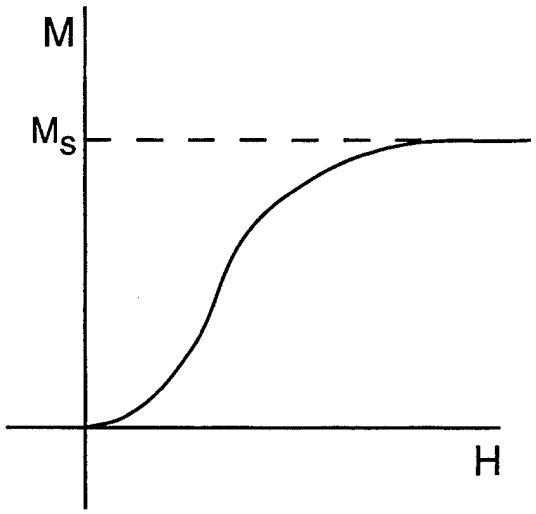

Figure 1. Initial Magnetization Curve.

mechanisms in the magnetic material. This behavior can be shown graphically through an $H - M$ magnetization curve, figure 1, where H is the applied magnetic field and M is the additional magnetic field created by the material. M is conventionally referred to as the magnetization of the material. In a vacuum, the perfect nonmagnetic material, the magnetization M has a value of zero for any applied field H. Once the material reaches its saturation magnetization M_s, further increases in applied field H do not increase the magnetization value.

The magnetization M is written in terms of the applied field H as

$$M = (\bar{\mu}_r - 1)H, \tag{1}$$

where $\bar{\mu}_r$ is a dimensionless material parameter called the relative magnetic permeability, or simply "permeability." The relative permeability of a vacuum is unity. Equation 1 is actually a simplification of the general magnetization curve, since clearly from figure 1 the magnetization M is not linearly related to the applied field H. The relationship can be written more generally as

$$M(H) = (\bar{\mu}_r(H) - 1)H. \tag{2}$$

In magnetic material property tables, permeability is rarely tabulated as a function of the applied field H. Instead, the initial permeability (at low H) or some characteristic permeability averaged over a range of H is given.

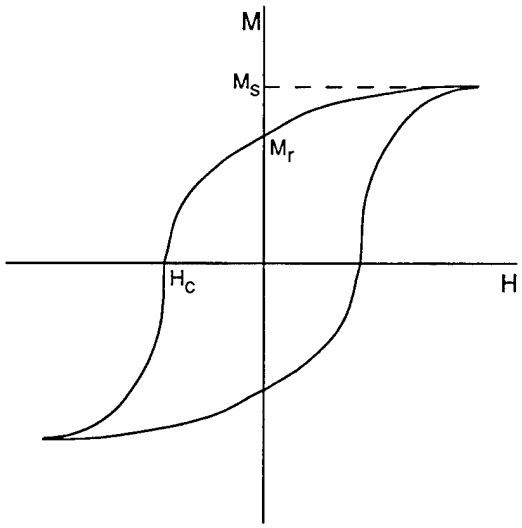

Figure 2. Typical DC Hysteresis Curve.

In an alternating magnetic field, the magnetization of the material typically demonstrates hysteretic behavior as shown in figure 2. This figure represents the saturation hysteresis loop, where the saturation magnetization of the material is reached. The magnetization at zero applied field is called the remanance M_r and the applied field necessary to reduce the magnetization to zero is called the coercivity H_c. These values are also frequently tabulated in magnetic property data tables. Unless otherwise noted, these values are measured in a steady (zero frequency) magnetic field.

We will now formalize our language for discussing magnetic materials and fields. In this report we will use the terminology "magnetic field" to refer to B (in Teslas, where 1 T = 1 We/m^2 = 1 J/A m^2), which is proportional to the sum of the applied "H" field (we choose not to name this quantity) and the material magnetization M, or

$$B = \mu_o (H + M), \tag{3}$$

where μ_o is the magnetic permeability of free space, whose exact value is defined as

$$\mu_o = 4\pi \times 10^{-7} \text{ H/m}. \tag{4}$$

The units of the magnetic permeability are Henries per meter, which can be rewritten as 1 H/m = 1 N/A^2. The magnetic field B is essentially the total magnetic field, created by the sum of the applied field H and the material magnetization M. Under our convention the units of B differ from the units of H and M. (This difference in units is not meant to imply any special

physical difference between the character of B relative to H and M. Rather, it exists mainly as an artifact of historical convention.) Equation 3 can be rewritten in terms of the relative magnetic permeability as

$$B = \mu_o \bar{\mu}_r H. \tag{5}$$

Since the magnetization M, and therefore the magnetic field B, are not linearly related to the applied field H, this equation can be written more generally as

$$B(H) = \mu_o \bar{\mu}_r(H) H. \tag{6}$$

In all of our equations we have written H, M, and B as scalar quantities. They are more correctly written in vector form, where equation 5 becomes

$$B_i = \mu_o (\bar{\mu}_r)_{ij} H_j. \tag{7}$$

Indicial notation is used here with the Einstein summation convention. Note that, in general, the relative permeability of a material is a tensor. For the remainder of this paper we will assume isotropic materials and uniform unidirectional magnetic fields, so that the scalar forms of the magnetic equations can be used.

Section 2.2 will require use of the magnetic flux Φ, defined for some conductive loop perpendicular to a magnetic field as the product of the magnetic field strength and the loop area, or

$$\Phi = B A_l, \tag{8}$$

where A_l is the area enclosed by the current loop. The magnetic flux is in many ways a contrived quantity that is only meaningful when used within the context of Faraday's law, which will be presented in equation 13. (A word of caution to readers who are new to electromagnetic field [EMF] theory and terminology. Note that the "magnetic field" B is equal to the "magnetic flux" Φ normalized by some area through which it acts. This convention is exactly opposite to the normal definition of "flux" in physics and engineering. If instead the following terminology

was used

$$B \rightarrow \text{magnetic flux [We/m}^2\text{]},$$
$$\Phi \rightarrow \text{magnetic flow [We]},$$
$$H \rightarrow \text{magnetic field strength [A/m]},$$

then the vocabulary would be more consistent with other branches of physics. Some authors have endeavored towards this end by calling H the magnetic field strength, Φ the magnetic flux, and B the magnetic flux density. However, the resulting language is perhaps even more confusing than the original.)

2.2 Eddy Current Heating. A conductive material placed in an alternating magnetic field has alternating currents induced within it. These currents generate heat in the material due to Joule (resistive) effects, a phenomenon known as eddy current heating.

Consider a spherical particle of radius R_o and resistivity ρ_Ω in the presence of a uniform periodic magnetic field of strength

$$B = B_p \sin \omega t, \tag{9}$$

where B_p is the field amplitude and ω is the frequency of the field (in radians per second). By assuming a uniform field and a spherical particle, the exact direction of the field is not important. However, for calculation purposes we will define a cylindrical coordinate system such that the magnetic field acts in the $-z$ direction.

Because induction heating is a volumetric phenomenon, we will be performing a volumetric integration. The discretization of the geometry is shown in Figure 3, for a slice of the sphere in the $r - \theta$ plane. We will use the notation $R(z)$ to represent the radius of the slice, where

$$R(z) = \sqrt{R_o^2 - z^2}. \tag{10}$$

The resistance R_Ω of the circumferential strip of width dr and height dz is

$$R_\Omega = \rho_\Omega \frac{\text{length}}{\text{cross-sectional area}} = \rho_\Omega \frac{2\pi r}{dr\,dz}. \tag{11}$$

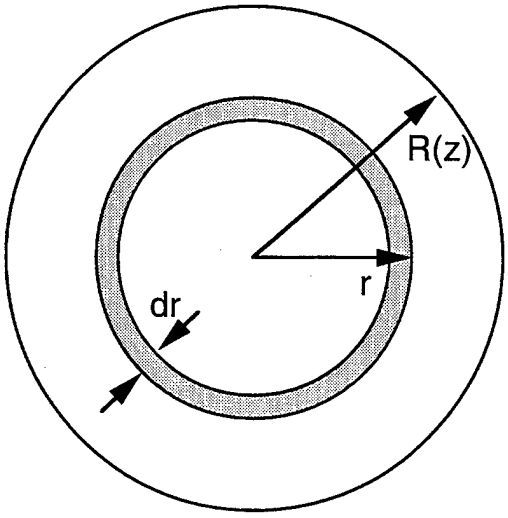

Figure 3. Discretization of Sphere for Eddy Current Model.

The magnetic flux Φ for this strip is defined as the product of the magnetic field strength and the area enclosed by the strip

$$\Phi = (B_p \sin \omega t)\, \pi r^2. \tag{12}$$

Faraday's Law states that the EMF generated in a current loop is proportional to the rate of change of the magnetic flux, or

$$V = -\frac{d\Phi}{dt}. \tag{13}$$

For our periodic magnetic flux, the induced EMF is also periodic

$$V = -\pi r^2 \omega \left(B_p \cos \omega t\right). \tag{14}$$

Note that the induced EMF is exactly out of phase with the magnetic flux, and its highest values occur when the magnetic flux is zero but the rate of change of the magnetic flux is maximized.

The power consumed due to Joule heating in the circumferential strip is

$$dP = \frac{V^2}{R_\Omega}, \tag{15}$$

$$= \frac{\left(\pi r^2 \omega \left[B_p \cos \omega t\right]\right)^2}{\rho_\Omega \frac{2\pi r}{dr dz}}, \tag{16}$$

$$= \frac{\pi r^3 \omega^2 B_p^2 \cos^2 \omega t}{2\rho_\Omega} dr dz. \tag{17}$$

Taking the time average of this instantaneous power function gives

$$dP = \frac{\pi r^3 \omega^2 B_p^2}{4\rho_\Omega} dr dz. \tag{18}$$

The total power consumed over the entire strip is

$$P = \int dP, \tag{19}$$

$$= 2 \int_0^{R_o} \int_0^{R(z)} \frac{\pi r^3 \omega^2 B_p^2 \cos^2 \omega t}{4\rho_\Omega} dr dz, \tag{20}$$

$$= \frac{\pi \omega^2 B_p^2}{2\rho_\Omega} \int_0^{R_o} \int_0^{R(z)} r^3 dr dz, \tag{21}$$

$$= \frac{\pi \omega^2 B_p^2}{2\rho_\Omega} \int_0^{R_o} \frac{1}{4} R(z)^4 dz. \tag{22}$$

Using equation 10,

$$P = \frac{\pi \omega^2 B_p^2}{8\rho_\Omega} \int_0^{R_o} (R_o^2 - z^2)^2 dz, \tag{23}$$

$$= \frac{\pi \omega^2 B_p^2}{8\rho_\Omega} (\frac{8}{15} R_o^5), \tag{24}$$

$$= \frac{\pi \omega^2 B_p^2}{15\rho_\Omega} R_o^5. \tag{25}$$

Normalizing this quantity by the volume of the sphere gives

$$P = \frac{\pi \omega^2 B_p^2 R_o^2}{20\rho_\Omega}. \tag{26}$$

This formula can be re-expressed in terms of the frequency $f \equiv \omega/2\pi$ (in cycles per second) and sphere diameter D_o as

$$\boxed{P_e = \frac{(\pi f B_p D_o)^2}{20\rho_\Omega},} \tag{27}$$

where we have added the subscript e to distinguish this quantity as the volume-averaged eddy current power.

A number of important trends can be observed from equation 27. The eddy current power increases with frequency squared and sphere diameter squared, while it decreases with increasing resistivity. Therefore we know that the eddy current power can be minimized by using lower frequencies, smaller particles, and higher resistivity materials.

2.3 Hysteresis Heating. In the presence of a magnetic field, a magnetic material undergoes a process of microstructural alignment. The mechanisms involved in this realignment include magnetization rotation and domain wall motion. In most polycrystalline materials, domain wall motion is the "easier" process, and is responsible for most of the magnetization changes within the material. Domain wall motion is a highly irreversible process, so that significant energy losses are associated with material magnetization. In an alternating magnetic field, these losses occur continuously over time, resulting in power consumption which takes the form of heating in the material.

Figure 4 shows a typical $H - M$ hysteresis curve for a magnetic material. By gradually imposing a field H_p, reversing the field to $-H_p$, and then reimposing the field H_p, the magnetization M follows this hysteresis curve. The exact shape of the curve is a function of the susceptor material, the susceptor material temperature, and the frequency of the applied field. If the potential energy of the system is defined as $\mu_o MH$, then the total energy lost during one complete hysteresis cycle, per unit volume of material, is

$$E_h = \mu_o \oint H dM. \tag{28}$$

If an alternating current is applied to the material, then the hysteresis loop is traversed once per cycle, so that the power consumed is

$$\boxed{P_h = f E_h.} \tag{29}$$

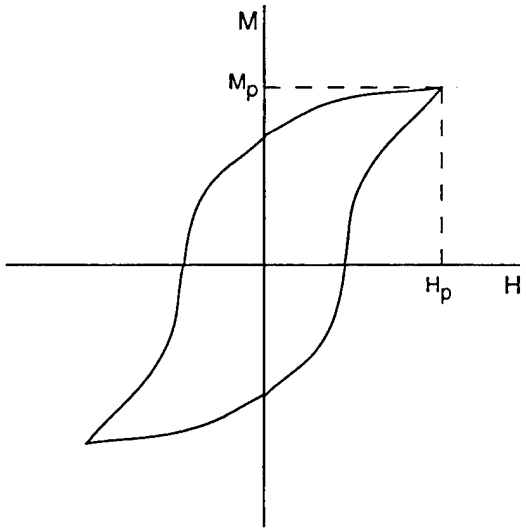

Figure 4. General Hysteresis Curve.

This equation is exact, provided the hysteresis energy density is known exactly for the processing conditions (temperature, imposed field amplitude, frequency).

For a specific material system, the best way to implement equation 29 is to measure the hysteresis curve for the material at the desired frequency, amplitude, and temperature. However, it is rare to find the exact desired hysteresis curve for a given material in the literature. Therefore methods are needed for estimating a specific hysteresis curve area based on available information.

DC saturation curves for the three specific materials under consideration for susceptor particles are given in section 4. No AC hysteresis curves for these materials could be found in the literature. Although in many materials the hysteresis energy density is frequency-dependent [23, 24], the best estimate we can make with the available information is frequency-independent hysteresis energy density equal to the DC hysteresis energy density.

Saturation hysteresis curves are directly useful if the applied field necessary to achieve saturation is less than or equal to the actual field strength which can be applied with feasible induction manufacturing and repair equipment. This situation is common with soft magnetic materials. If the applied field necessary to achieve saturation is much greater than the feasible equipment field strength, as is the case with hard magnetic materials, then magnetic saturation in the material is never reached. In this case it is necessary to approximate a minor hysteresis loop for the material based on its major hysteresis loop.

For a saturation hysteresis loop, we can write the saturation hysteresis energy density as

$$E_{hs} = \beta \mu_o M_s H_s, \tag{30}$$

where H_s is the field strength required to mostly saturate the material and β is a constant bounded by [0,1]. It is reasonable to assume that minor hysteresis loops are shaped similarly to the major loops, only scaled according to the applied field strength. This assumption has two consequences. First, β is constant, so any minor hysteresis loop can be written as

$$E_h = \beta \mu_o M_p H_p. \tag{31}$$

Secondly, the peak magnetization decreases linearly with the applied field strength, or

$$\frac{M_p}{M_s} \sim \frac{H_p}{H_s}. \tag{32}$$

Combining equations 30 and 31 yields

$$E_h = E_{hs} \frac{M_p}{M_s} \frac{H_p}{H_s} \tag{33}$$

which, when combined with equation 32, gives

$$E_h = E_{hs} \left(\frac{H_p}{H_s} \right)^2. \tag{34}$$

For all field strengths greater than H_s, E_h will be equal to E_{hs}. Therefore we can write equation 34 more generally as

$$E_h = \begin{cases} E_{hs} \left(\frac{H_p}{H_s} \right)^2 & \text{if} H_p < H_s, \\ E_{hs} & \text{if} H_p \geq H_s. \end{cases} \tag{35}$$

For our derivations in section 3.1, we will find it useful to write an alternate expression for the hysteresis energy density. We define a hysteresis permeability $\bar{\mu}_h$ as

$$\bar{\mu}_h \equiv 1 + \frac{E_{hs}}{\mu_o H_s^2} \tag{36}$$

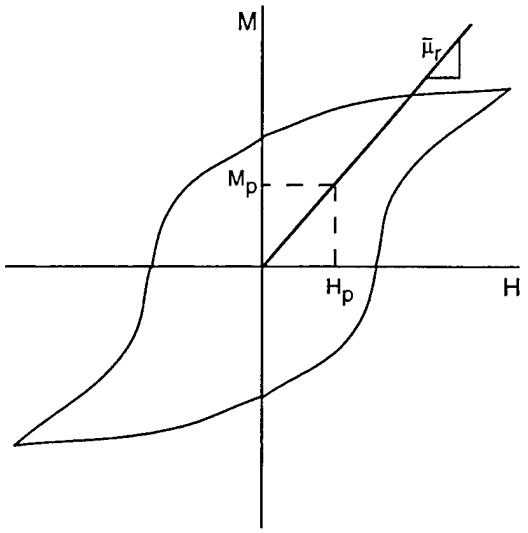

Figure 5. Approximation of the Initial Permeability from a Saturation Hysteresis Curve.

so that

$$E_{hs} = \mu_o(\bar{\mu}_h - 1)H_s^2. \tag{37}$$

$\bar{\mu}_h$ is essentially the proportionality constant between E_{hs} and H_s^2, and can be calculated from a measured saturation hysteresis loop. We have chosen to express this hysteresis constant in a form analogous to a relative magnetic permeability, because it simplifies later derivations and has a value of unity for non-lossy materials. Equation 34 can be rewritten as

$$E_h = \mu_o(\bar{\mu}_h - 1)H_p^2. \tag{38}$$

Therefore, the complete hysteresis energy model of equation 35 can be implemented for a material if $\bar{\mu}_h$ and H_s are known.

We will also find it necessary to estimate the true magnetic permeability of a material from its saturation hysteresis loop. This parameter will be used in derivations which need to estimate the magnetic field strength produced by a material for a given applied field strength. Since permeability is actually a function of applied field strength (equation 6), we need some sort of average permeability value. Furthermore, we will need to estimate this value based on a given saturation hysteresis curve. The approach we will use is to graphically estimate the average permeability, as shown in Figure 5.

2.4 Field Penetration Depth. Induction heating is a volumetric effect. The eddy current analysis in section 2.2 assumed a uniform magnetic field throughout the particle. However, the induced currents in the particle create a magnetic field which opposes the applied magnetic field, a phenomenon known as the shielding effect. Typically, the net magnetic field is highest at the surface of the susceptor and decreases exponentially with depth. The penetration depth is usually expressed in terms of a skin depth, δ, which can be calculated by [25]

$$\delta = \sqrt{\frac{\rho_\Omega}{\pi \mu_o \bar{\mu}_r f}}. \tag{39}$$

The skin depth is defined as the distance at which the magnetic field has been reduced to around 37% $(1/e)$ of its surface value. If the skin thickness is less than the particle size, then shielding effects are important.

2.5 Induction Head. Induction heating equipment typically consists of a power supply, an induction head, and a cooling system. The power supply sends current through the induction head, which is made of a winding of low-resistivity material such as copper. The shape of the head, its position relative to the susceptor, and the current flowing through the head determine the magnetic field applied to the susceptor. Power is consumed through heating of the susceptor, due to eddy and hysteresis losses, and through resistive heating in the head. The resistance of the head must be minimized to reduce head losses. Because of the high currents necessary to induce significant magnetic fields, the induction head is often cooled through water or air cooling. The most common approach is to make the induction head out of copper tubing, and continually circulate cooling water through the head.

In order to model the power loss in the head, the resistance of the head must be calculated through

$$R_\Omega = \rho_\Omega \frac{L_{ih}}{A_{ih}}, \tag{40}$$

where L_{ih} and A_{ih} are the length and cross-sectional area of the induction head, respectively. The power loss in the head, $P = I^2 R_\Omega$, is then

$$P_{ih} = I^2 \rho_\Omega \frac{L_{ih}}{A_{ih}}. \tag{41}$$

For a given current and head resistance, this formula allows calculation of the power consumed by the head. This value can be used to determine the necessary cooling system capacity.

We must also calculate the magnetic field produced by a typical induction head. The magnetic field produced by a single current loop of radius R at a distance z along the centerline of the loop is [26]

$$B = \frac{\mu_o I}{2} \frac{R^2}{(R^2 + z^2)^{3/2}}. \tag{42}$$

A typical "pancake-coil" induction head consists of a set of concentric current loops. The magnetic field produced by this head can be calculated by summing the contributions of each loop as calculated by equation 42.

2.6 Heat Transfer in Particulate Film. We will use the terminology "particulate film" to refer to both thermoplastic films and adhesives loaded with volumetrically-heating particles because, neglecting heats of fusion and reactive exotherms, the heat transfer models are identical for both cases. These secondary heat transfer effects are expected to be insignificant for this order-of-magnitude feasibility study, but need to be incorporated into any future quantitative modeling efforts.

Since the particles and the distance between particles are small, we will use a very simple lumped analysis for modeling the heat transfer in the particulate film. For a film consisting of a volume fraction v_f of particles of density ρ and specific heat c_p dispersed in a matrix of density $\tilde{\rho}$ and specific heat $\tilde{c}_p$, the power required to heat the film over a temperature change $\triangle T$ in a time $\triangle t$ is

$$P_f = \frac{\triangle T}{\triangle t} \left(v_f \rho c_p + (1 - v_f) \tilde{\rho} \tilde{c}_p \right), \tag{43}$$

where P_f is the power consumed in the film, per volume of film.

This heat transfer model assumes that the heat which is generated within the particles is immediately and uniformly distributed over the entire film. This assumption is only valid if the spacing between the particles is sufficiently small such that heat can be transferred across that distance in a time much shorter than the process time. We can calculate the critical spacing between the particles by calculating the characteristic conduction length scale for the film, L_c

$$L_c = \sqrt{\alpha_c \triangle t}, \tag{44}$$

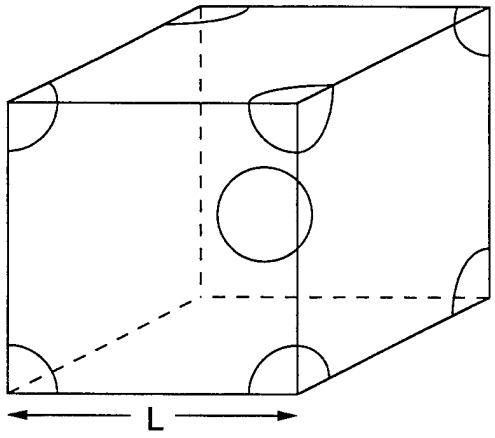

Figure 6. Particle Dispersion Geometry for Characteristic Conduction Length Calculation.

where α_c is the thermal conductivity of the film. For a body-centered cubic arrangement of spherical particles, Figure 6, the particle volume fraction can be expressed as

$$v_f = \frac{2\frac{1}{6}\pi D_o^3}{L^3}, \tag{45}$$

where L is the particle spacing along the primitive cell edges. Since heat is only generated within the particles, the characteristic conduction length is roughly the distance L between particles. Equating $L = L_c$, combining equations 44 and 45, and rearranging yields

$$D_o = \left(\frac{3}{\pi}\right)^{1/3} v_f^{1/3} \sqrt{\alpha_c \triangle t}. \tag{46}$$

Taking $3/\pi \sim 1$ gives

$$D_c = v_f^{1/3} \sqrt{\alpha_c \triangle t}. \tag{47}$$

For a given particle volume fraction v_f and film thermal diffusivity α_c, the particle size must be less than D_c in order to keep the characteristic conduction times less than $\triangle t$.

3. Design Parameters

Now that the relevant physics for this problem have been modeled, design criteria can be derived which place bounds on acceptable material properties and equipment capabilities for processing.

3.1 Eddy Heating to Hysteresis Heating Ratio. For automatic temperature control through Curie temperature effects, the eddy heating in the particles must be significantly less than the hysteresis heating in the particles. Using equations 27 and 29, this ratio is

$$\boxed{R_p = \frac{P_e}{P_h} = \frac{(\pi B_p D_o)^2 f}{20 \rho_\Omega E_h}.} \tag{48}$$

This relation for the heating ratio R_p is its most accurate form, and should be used whenever possible.

Since E_h is dependent on B_p, equation 48 is not in its most primitive form. Using equations 5 and 38 we can write

$$\frac{B_p^2}{E_h} = \frac{(\mu_o \bar{\mu}_r H_p)^2}{\mu_o (\bar{\mu}_h - 1) H_p^2}, = \mu_o \frac{\bar{\mu}_r^2}{\bar{\mu}_h - 1}. \tag{49}$$

Using this relationship to eliminate B_p and E_h from equation 48 yields

$$R_p = \frac{\pi^2}{20} \frac{D_o^2 f}{\rho_\Omega} \mu_o \frac{\bar{\mu}_r^2}{\bar{\mu}_h - 1}. \tag{50}$$

Taking $\pi^2/20 \sim 1$ the power ratio can be written as

$$R_p = \mu_o D_o^2 \left(\frac{\bar{\mu}_r^2}{\bar{\mu}_h - 1} \frac{1}{\rho_\Omega} \right) f \tag{51}$$

or

$$\boxed{R_p = \mu_o D_o^2 \Upsilon_1 f,} \tag{52}$$

where

$$\Upsilon_1 = \frac{\bar{\mu}_r^2}{\bar{\mu}_h - 1} \frac{1}{\rho_\Omega}. \tag{53}$$

Υ_1 is the relevant material parameter for determining the ratio of eddy heating to hysteresis heating. Note that the power ratio decreases (less eddy heating) for materials with higher resistivities, smaller particles, and lower frequencies. The power ratio becomes infinite for a hysteresis permeability of 1. This case corresponds to a material with no hysteresis losses.

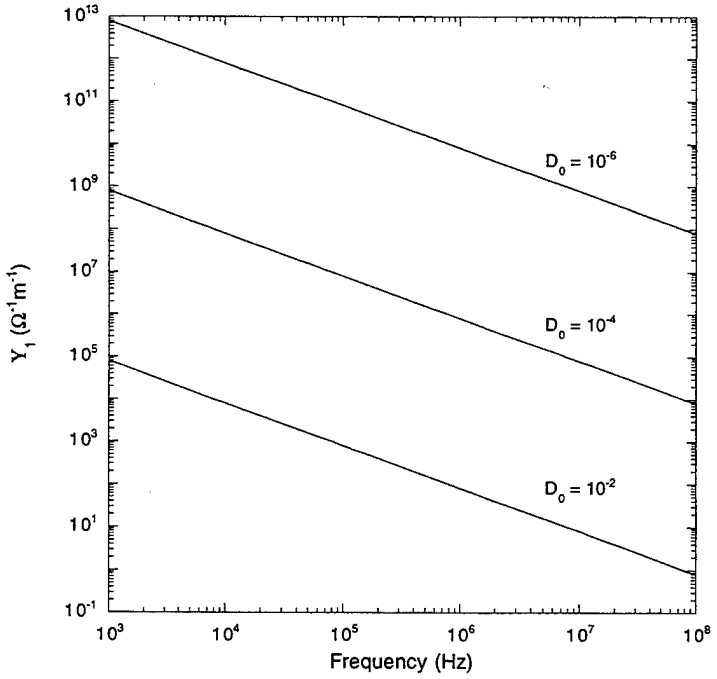

Figure 7. Power Ratio Plot.

We can use equation 52 to create a guideline for designing an induction heating process with negligible eddy heating. We will impose the (somewhat arbitrary) condition that eddy heating is insignificant if $R_p < 0.01$. We can then plot D_o as a function of Υ_1 and f for this value of R_p. The resulting plot, Figure 7, shows the limiting particle sizes for insignificant eddy heating as a function of the material and imposed frequency.

3.2 Dimensionless Penetration Depth. In section 2.4 we presented the relationship for the magnetic field penetration depth as a function of the material parameters and applied field. If the penetration depth is comparable to or less than the particle dimension, then shielding effects are significant. In this case both our eddy and hysteresis models will be inaccurate and can no longer be applied, since they both assumed a uniform applied field. The actual field inside the particle will be reduced due to shielding effects, and heating will be diminished. Therefore we wish to keep the particle radius less than the penetration thickness. Defining a dimensionless penetration thickness ratio $R_s = 2\delta/D_o$, and using equation 39, we can write

$$R_s = \frac{2}{D_o}\sqrt{\frac{\rho\Omega}{\pi\mu_o\bar{\mu}_r f}}. \tag{54}$$

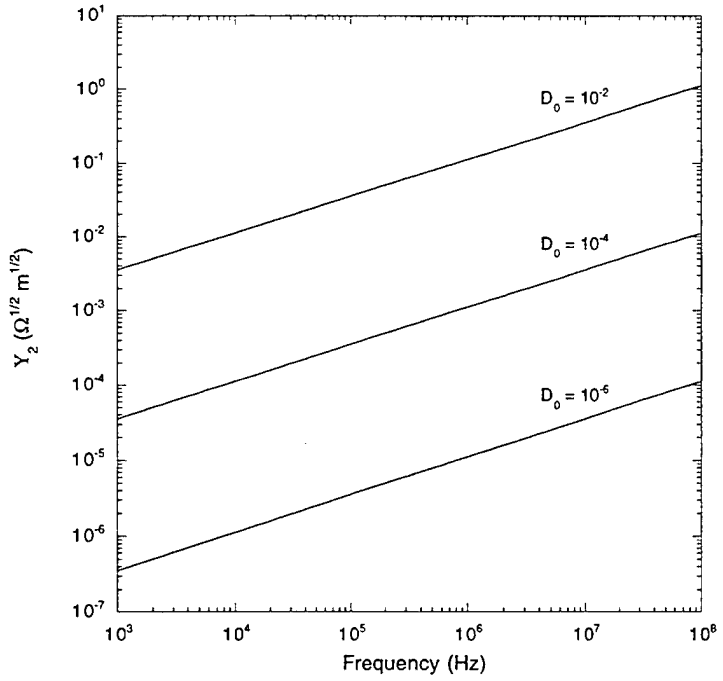

Figure 8. Dimensionless Penetration Thickness Plot.

If the dimensionless penetration thickness is large then shielding effects are insignificant. Since both heating power and shielding effects increase as frequency increases, shielding mechanisms will probably provide an upper bound on the feasible process frequency.

Taking $2/\sqrt{\pi} \sim 1$, equation 54 can be rewritten as

$$\boxed{R_s \sim \mu_o^{-1/2} D_o^{-1} \Upsilon_2 f^{-1/2},} \tag{55}$$

where

$$\Upsilon_2 = \sqrt{\frac{\rho_\Omega}{\bar{\mu}_r}}. \tag{56}$$

Υ_2 is the relevant material parameter for determining the dimensionless penetration depth. We can use this equation to create a guideline for designing an induction heating process with negligible shielding effects. We will impose the (somewhat arbitrary) condition that shielding is insignificant if $R_s > 10$. We can then plot D_o as a function of Υ_2, and f for this value of R_s. The resulting plot, Figure 8, shows the limiting particle sizes for insignificant shielding as a function of the material and imposed frequency.

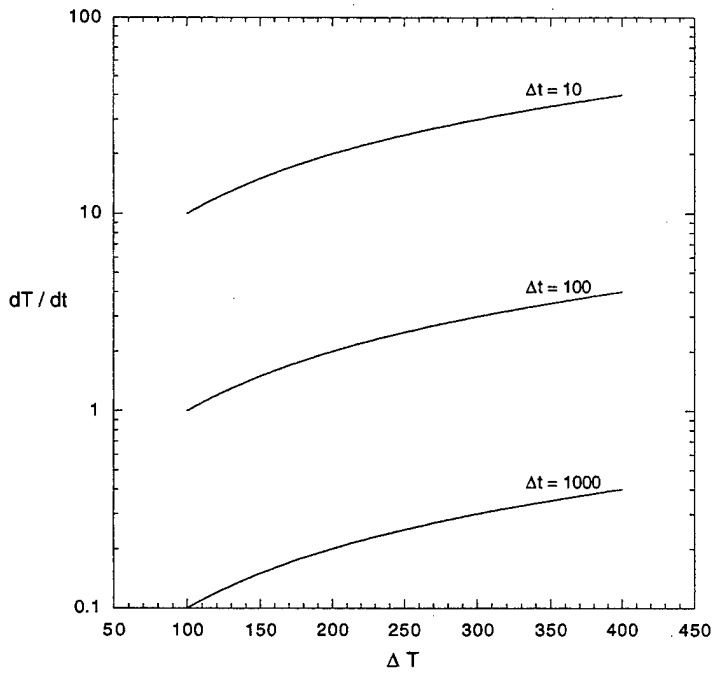

Figure 9. Characteristic Heating Rates.

3.3 Heating Rates. The time necessary to reach the processing temperature must be small enough to allow for rapid bonding and repair. We can rewrite equation 43 as

$$\frac{dT}{dt} \cong v_f P_h \left(v_f \rho c_p + (1 - v_f)\tilde{\rho}\tilde{c}_p\right)^{-1}. \tag{57}$$

The term dT/dt is the characteristic heating rate and $v_f P_h$ is the particle heating power due to hysteresis effects only, assuming negligible eddy heating. The extra factor of v_f is included because the hysteresis heating is generated only in the film volume occupied by the particles. Combining this equation with equation 29 and rearranging yields

$$\boxed{\frac{dT}{dt} \cong f\frac{E_h}{\rho c_p}\left(1 + \left(\frac{1}{v_f} - 1\right)\frac{\tilde{\rho}\tilde{c}_p}{\rho c_p}\right)^{-1}.} \tag{58}$$

This equation allows us to calculate the characteristic heating rate for a given material, particulate volume fraction, and applied field frequency. Figure 9 shows characteristic heating rates for different heating times and temperature rises. The range of $100° - 400°$C encompasses the expected range of processing temperature changes for elevated-temperature adhesives and engineering thermoplastics. A heating time of 100 s is considered reasonable. Therefore we need to achieve heating rates of at least $1° - 10°$C/s.

A number of important trends are revealed by equation 58. The heating rate is proportional to the field frequency. Therefore increasing the frequency by an order of magnitude should also increase the heating rate by an order of magnitude. Increasing the hysteresis loop energy density also proportionally increases the heating rates. However, it is very easy to increase the field frequency by orders of magnitude through equipment selection and control, while there is no systemic means of increasing hysteresis energy density.

The effect of particle volume fraction on heating rates can be investigated by writing the ratio of the heating rate for general v_f to the particle heating rate ($v_f = 1.0$) as

$$\frac{(dT/dt)_{v_f}}{(dT/dt)_p} = \frac{1}{1 + (1/v_f - 1)(\tilde{\rho}\tilde{c}_p/\rho c_p)}. \tag{59}$$

This equation gives the dimensionless heating rate as a function of the particle volume fraction and the specific heat ratio $\tilde{\rho}\tilde{c}_p/\rho c_p$. Figure 10 shows the dimensionless heating rate as a function of volume fraction for three different specific heat ratios. Note that when the matrix specific heat is less than the particle specific heat ($\tilde{\rho}\tilde{c}_p/\rho c_p = 0.1$), which is the case most common for magnetic particles in polymer matrices, significant changes in heating rate with volume fraction are noted at low particle volume fractions. However, at higher volume fractions, little change in heating rate is noted as particle volume fraction is increased. This behavior is advantageous, allowing significant film heating with relatively low particle volume fractions.

3.4 Curie Temperature. For systems with negligible eddy heating, the Curie temperature represents the dwell temperature of the material during induction heating, assuming the inductive heating power is sufficient to overcome thermal losses and heat the susceptor to this temperature. Since the processing temperature of most elevated-temperature adhesives and engineering thermoplastics is between 100° and 400°C, only materials with Curie temperatures in this range should be considered for the particulates.

4. Calculations for Specific Material Systems

In this section we perform quantitative calculations of the design variables for specific equipment and material configurations. In section 4.1, equipment capabilities are quantified and some preliminary heat transfer calculations are performed. Sections 4.2-4.4 then provide characteristic heating behaviors for three different materials: nickel, strontium ferrite, and nickel zinc ferrite, representing elemental ferromagnetic, hard ferrite, and soft ferrite magnetic materials, respectively.

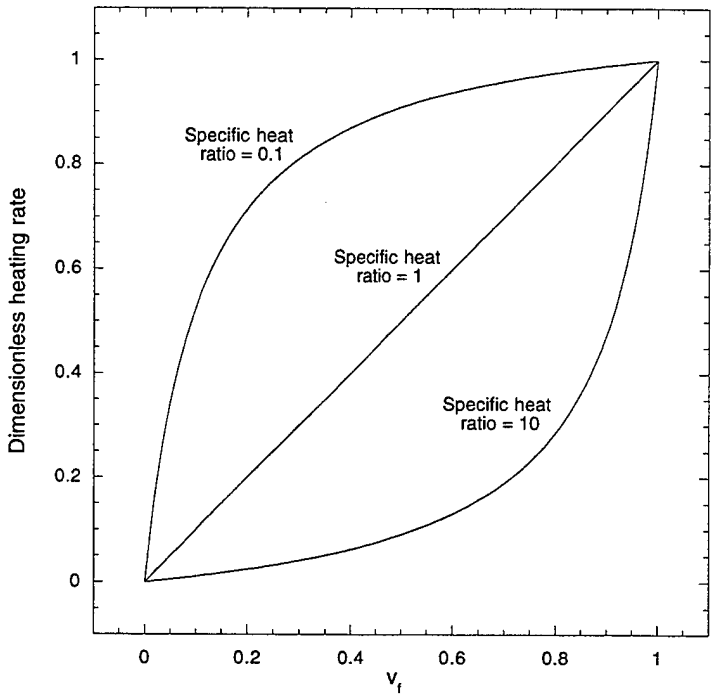

Figure 10. Dimensionless Heating Rates as a Function of Particle Volume Fraction v_f and Matrix/Particle Specific Heat Ratio $\tilde{\rho}\tilde{c}_p/\rho c_p$.

4.1 General Equipment and Matrix Properties. Although many induction coil geometries are possible, for our benchmarking purposes we will consider a standard 5-turn pancake coil made out of copper tubing with 10 mm outside diameter and 2 mm wall thickness. We will approximate the coil as 5 concentric circles of radius 2, 4, 6, 8, and 10 cm. The effective length and cross sectional area of this head are

$$L_{ih} = 2\pi(20 + 40 + 60 + 80 + 100) \text{ mm} \qquad A_{ih} = \frac{1}{4}\pi(10^2 - 6^2) \text{ mm}^2. \tag{60}$$

A typical induction unit passes 100 A of current. Using a copper resistivity value of 1.7×10^{-8} Ω m [27] and the resistive heating power equation, equation 41, the head consumes a total power of $P_{ih} = 6.4$ W. Since we expect to use power supplies with kW capacity, the power consumed by the head is negligible.

For our pancake coil geometry, and assuming the coil is located 2 cm above the susceptor material, equation 42 predicts a field strength of

$$B = 4.44 \times 10^{-5} I, \tag{61}$$

Table 1. Typical Polymer Matrix Thermophysical Properties.

Property	Value
Density ($\tilde{\rho}$)	1000 kg/m^3
Specific heat ($\tilde{c}_p$)	1000 J/kg K
Thermal conductivity ($\tilde{k}$)	0.2 W/m K

where I is in Amps, and B is in Teslas. For a current of 100 A, the magnetic field is $B = 4.44 \times 10^{-3}$ T. Converting this value to an H value using $H = B/\mu_o$, the field value is 3500 A/m. This value will be used as our maximum field strength in all subsequent calculations.

Commercial induction heating equipment usually operates in the range of 1 kHz to 10 MHz. However, higher frequency equipment can be manufactured if needed.

For our film heat transfer model, the thermal properties of the suspending medium are needed. These properties, typical for adhesives and engineering thermoplastics, are given in Table 1. Using these matrix properties as the overall film properties (a conservative estimate), and setting the characteristic conduction time as 1 s, equation 47 gives the critical particle diameter for uniform heating as

$$D_c = v_f^{1/3} \sqrt{\frac{\tilde{k} \triangle t}{\tilde{\rho} \tilde{c}_p}} = (4.47 \times 10^{-4}) v_f^{1/3} \text{ m}. \tag{62}$$

This critical particle diameter is plotted as a function of volume fraction in Figure 11. Note that even at particle volume fractions of only 1%, the critical particle diameter is $\sim$ 100 μm. According to this calculation, if the particles are less than 100 μm in diameter, heating throughout the film should be uniform. At higher volume fractions this critical particle size increases to $\sim$ 300 μm. Since this calculation is only guaranteed to be accurate within one or two orders of magnitude, it is probably best to use particles no larger than 1-10 μm.

4.2 Nickel (Elemental Ferromagnetic). Of the five elemental ferromagnetic materials, iron, cobalt, nickel, gadolinium, and dysprosium, nickel is the only one whose Curie temperature, 358°C, is within the bounds of thermoplastic processing. As a powder it is also readily available and inexpensive. Table 2 lists some of the relevant magnetic and thermophysical properties for nickel. Figure 12 shows a DC saturation hysteresis loop for 3 μm nickel powder, measured by Suwanwatana [28]. The magnetic properties in Table 2 were calculated from this DC hysteresis curve. E_{hs} is the area of the loop, H_s is applied field strength necessary

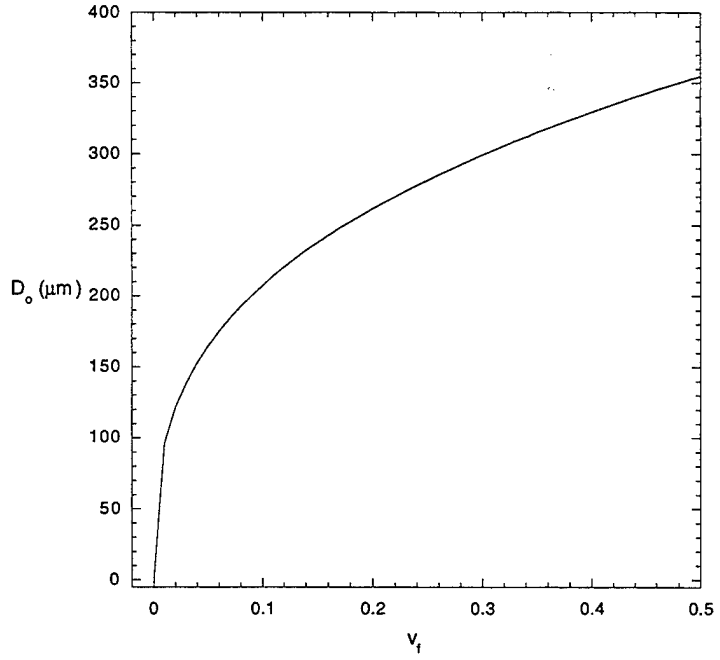

Figure 11. Critical Particle Diameter to Maintain Thermal Conduction Times on Order of 1 s, as a Function of Volume Fraction.

to mostly saturate the material, and $\bar{\mu}_r$ is measured graphically, as suggested in section 2.3. The $\bar{\mu}_r$ value of 8.0 suggests that at our expected maximum applied field strength, 3500 A/m, the material magnetization will be $B_p = 0.03$ T.

Using equation 56 and the values of ρ_Ω and $\bar{\mu}_r$ from Table 2, the penetration thickness material parameter Υ_2 has a value for nickel of

$$\Upsilon_2 = 9.2 \times 10^{-5}\ \Omega^{1/2}\mathrm{m}^{1/2}. \tag{63}$$

From Figure 8, we can see that for this value of Υ_2 skin effects may become important. For example, at 1 MHz, the particles must be smaller than 10 μm for shielding to be unimportant. At 100 MHz, the particles must be smaller than 1 μm.

Using equation 36 and the values of E_{hs} and H_s from Table 2, we calculate $\bar{\mu}_h = 2.0$. Substituting this value with the values of ρ_Ω and $\bar{\mu}_r$ into equation 53, the heating ratio parameter Υ_1 has a value for nickel of

$$\Upsilon_1 = 9.4 \times 10^{8}\ \Omega^{-1}\mathrm{m}^{-1}. \tag{64}$$

Table 2. Nickel Thermophysical and Magnetic Properties. All values above horizontal line from Ozisik [29] except electrical conductivity, from Weast [27]. All values below line determined graphically from Figure 12.

Property	Value
Density (ρ)	8900 kg/m^3
Specific heat (c_p)	430 J/kg K
Electrical resistivity (ρ_Ω)	6.8×10^{-8} Ω m
Curie temperature	358°C
Saturation hysteresis energy density (E_{hs})	7200 J/m^3
Saturation applied field (H_s)	75 kA/m
Effective relative magnetic permeability ($\bar{\mu}_r$)	8.0

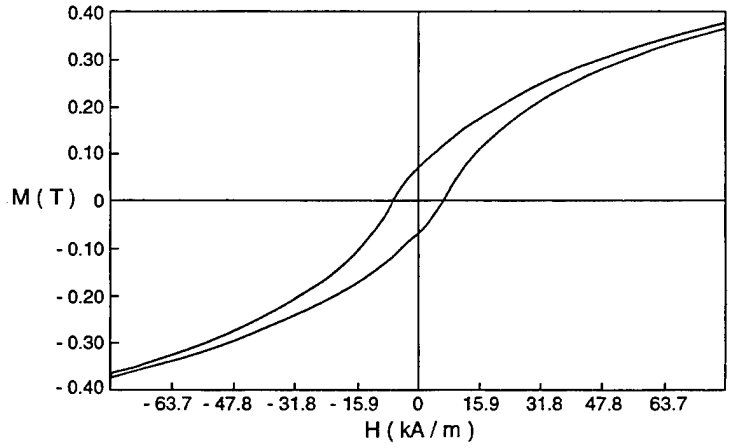

Figure 12. DC Saturation Hysteresis Curve for Nickel (from Suwanwatana [28]).

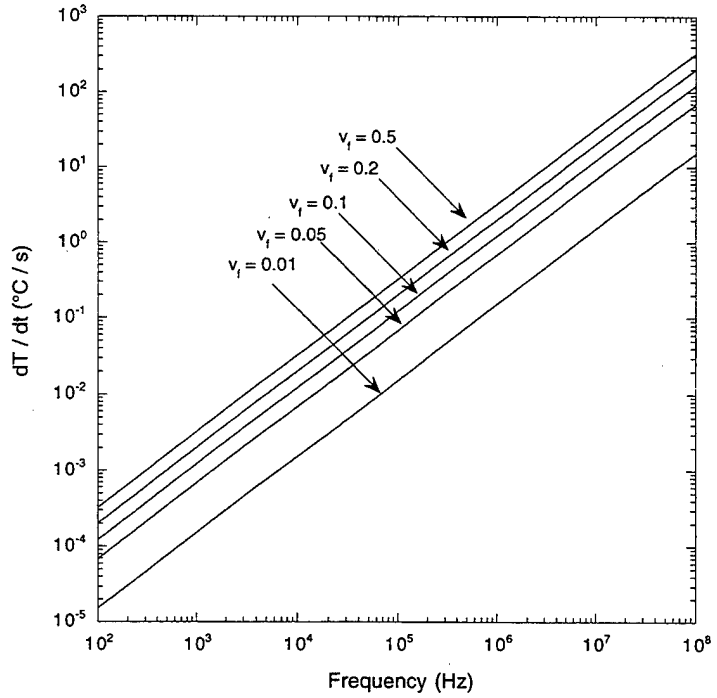

Figure 13. Heating Rate as a Function of Frequency for Nickel Particles of Various Volume Fractions in a Polymer Film.

From Figure 7, we can see that for this value of Υ_1 eddy heating becomes important for particles in the 1-10 μm size range for the range of frequencies we are considering. Eddy current heating may be important for particles which are larger than this size. Therefore, to ensure Curie temperature control, the particles should be kept smaller than 1 μm.

Using the hysteresis energy density approximation, equation 35, with the values of E_{hs} and H_s from Table 2 and a peak applied field magnitude of $H_p = 3500$ A/m, the hysteresis power density for nickel is 15.7 J/m^3. Combining this value with equation 58 and the material properties from Table 2, the heating rate for a particle / polymer film is

$$\frac{dT}{dt} \cong f(1.57 \times 10^{-5})\,(2.83 + 1/v_f)^{-1}\,. \tag{65}$$

Figure 13 shows the characteristic heating rate as a function of frequency for various volume fractions. Figure 14 shows the same information, but in terms of volume fractions for various heating rates. Figure 15 shows heating rates as a function of particle volume fraction for various frequencies. Note that the frequency must be at least 1 MHz to get reasonable heating rates.

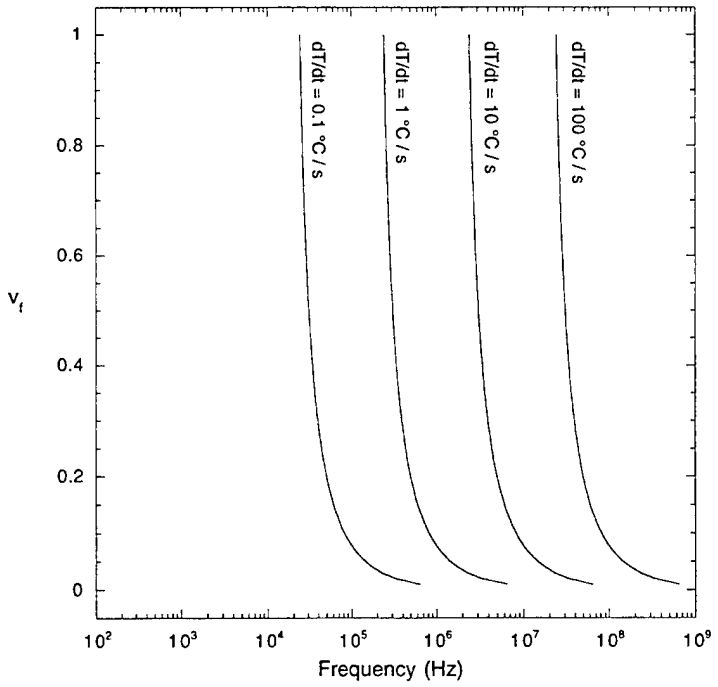

Figure 14. Nickel Particle Volume Fraction as a Function of Frequency for Various Film Heating Rates.

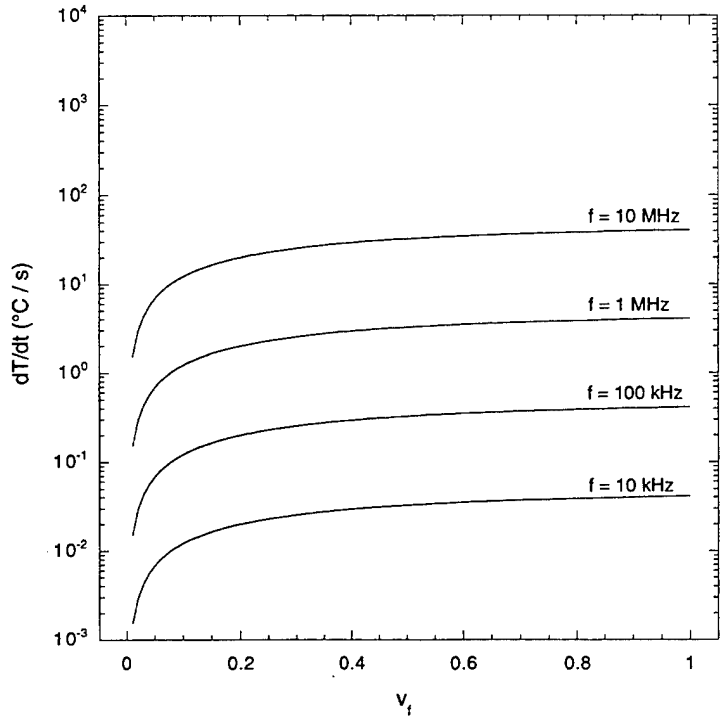

Figure 15. Heating Rates as a Function of Nickel Particle Volume Fraction for Various Frequencies.

Table 3. Strontium Ferrite Thermophysical and Magnetic Properties. All values above horizontal line from McCurrie [31] except specific heat, which is based on typical ferrite values. All values below line determined graphically from Figure 16.

Property	Value
Density (ρ)	4800 kg/m^3
Specific heat (c_p)	750 J/kg K
Electrical resistivity (ρ_Ω)	10^4 Ω m
Curie temperature	450°C
Saturation hysteresis energy density (E_{hs})	560 kJ/m^3
Saturation applied field (H_s)	600 kA/m
Effective relative magnetic permeability ($\bar{\mu}_r$)	1.7

4.3 Strontium Ferrite (Hard Ferrite). Strontium ferrite ($SrFe_{12}O_{19}$) is one of the most common commercial permanent magnet materials. It is cheap, readily available as a powder, and has a high coercivity typical of permanent magnet materials. The relevant thermophysical and magnetic properties for a typical strontium ferrite are shown in Table 3. Figure 16 shows a DC saturation hysteresis curve for Triton C strontium ferrite [30], developed in 1996 under a U.S. Army Small Business Innovative Research (SBIR) program with Triton Systems, Inc. (Chelmsford, MA) for the Weapons and Materials Research Directorate, U.S. Army Research Laboratory. The magnetic properties in Table 3 were calculated from this DC hysteresis curve. E_{hs} is the area of the loop, H_s is applied field strength necessary to mostly saturate the material, and $\bar{\mu}_r$ is measured graphically, as suggested in section 2.3. Note that the field necessary to reach saturation is approximately two orders of magnitude greater than the fields we expect to generate in our induction devices. The $\bar{\mu}_r$ value of 1.7 suggests that at our expected maximum applied field strength, 3500 A/m, the material magnetization will be $B_p = 0.003$ T.

Using equation 56 and the values of ρ_Ω and $\bar{\mu}_r$ from Table 3, the penetration thickness material parameter Υ_2 has a value for strontium ferrite of

$$\Upsilon_2 = 76.7\ \Omega^{1/2}\mathrm{m}^{1/2}. \tag{66}$$

From Figure 8, we can see that this value of Υ_2 does not even appear on the plot. For example, at a frequency of 100 MHz, shielding effects become important when D_o =70 cm, which is much larger than the particles we will be using.

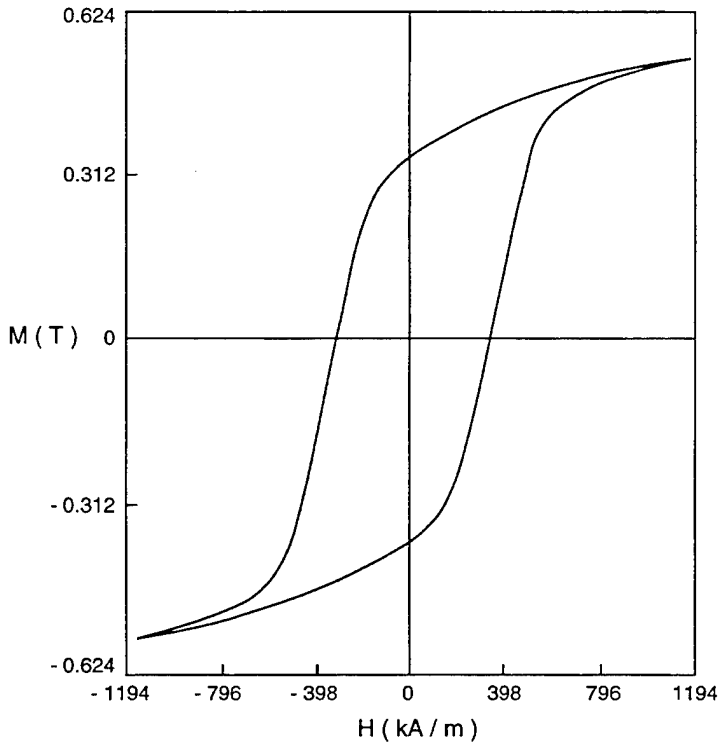

Figure 16. DC Saturation Hysteresis Curve for Strontium Ferrite (from Stark [30]).

Using equation 36 and the values of E_{hs} and H_s from Table 3, we calculate $\bar{\mu}_h = 2.2$. Substituting this value with the values of ρ_Ω and $\bar{\mu}_r$ into equation 53, the heating ratio parameter Υ_1 has a value for strontium ferrite of

$$\Upsilon_1 = 2.4 \times 10^{-4}\ \Omega^{-1}\mathrm{m}^{-1}. \tag{67}$$

This value of Υ_1 does not even appear in Figure 7. For example, at a frequency of 100 MHz, eddy heating becomes important when $D_o = 57$ cm. Therefore Curie temperature control should not be a problem for strontium ferrites.

Using the hysteresis energy density approximation, equation 35, with the values of E_{hs} and H_s from Table 3 and a peak applied field magnitude of $H_p = 3500$ A/m, the hysteresis power density for strontium ferrite is 19.1 J/m^3. Combining this value with equation 58 and the material properties from Table 3, the heating rate for a particle / polymer film is

$$\frac{dT}{dt} \cong f(1.91 \times 10^{-5})\,(2.60 + 1/v_f)^{-1}\,. \tag{68}$$

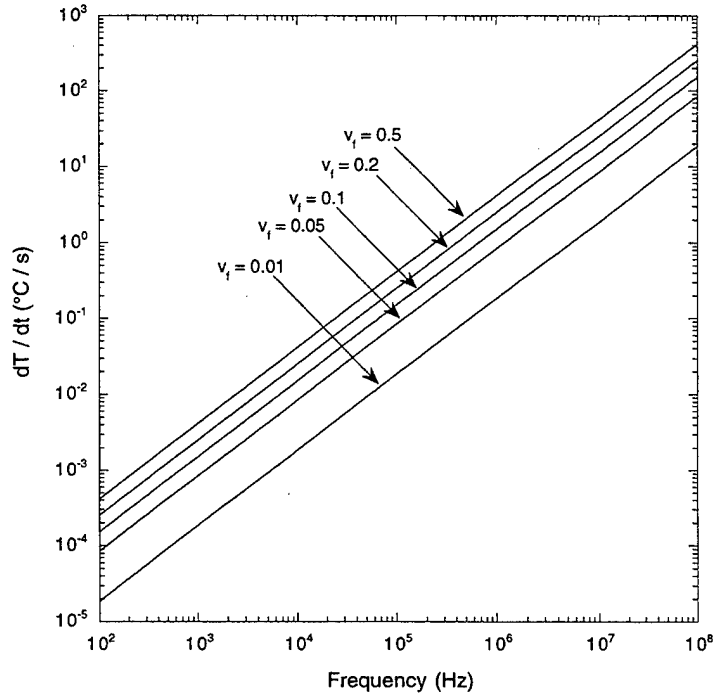

Figure 17. Heating Rate as a Function of Frequency for Strontium Ferrite Particles of Various Volume Fractions in a Polymer Film.

Figure 17 shows the characteristic heating rate as a function of frequency for various volume fractions. Figure 18 shows the same information, but in terms of volume fractions for various heating rates. Figure 19 shows heating rates as a function of particle volume fraction for various frequencies. The heating rates are similar to those observed in nickel, with frequencies of 1 MHz or higher required to reach 1°C/s.

4.4 Nickel Zinc Ferrite (Soft Ferrite). Nickel zinc ferrite ($Ni_{1-x}Zn_xFe_2O_4$) is a soft ferrite which is used extensively in transformer cores, mostly due to its high permeability and "low" hysteresis losses. NiZn ferrite was chosen for this study as a representative soft ferrite because its Curie temperature can be customized from 100°-600°C by varying the ratio of nickel to zinc in the material as shown in Figure 20 [32]. Snelling [33] provides extensive property listings and hysteresis curves for various NiZn ferrite grades. We will choose a grade of NiZn with a large coercivity, grade B5 from Snelling. The relevant thermophysical and magnetic properties for a typical NiZn ferrite are given in Table 4. Figure 21 shows a DC saturation hysteresis loop for this material. The magnetic properties in Table 4 were calculated from this DC hysteresis curve. E_{hs} is the area of the loop, H_s is applied field strength necessary to mostly saturate the material, and $\bar{\mu}_r$ is measured graphically, as suggested in section 2.3. The

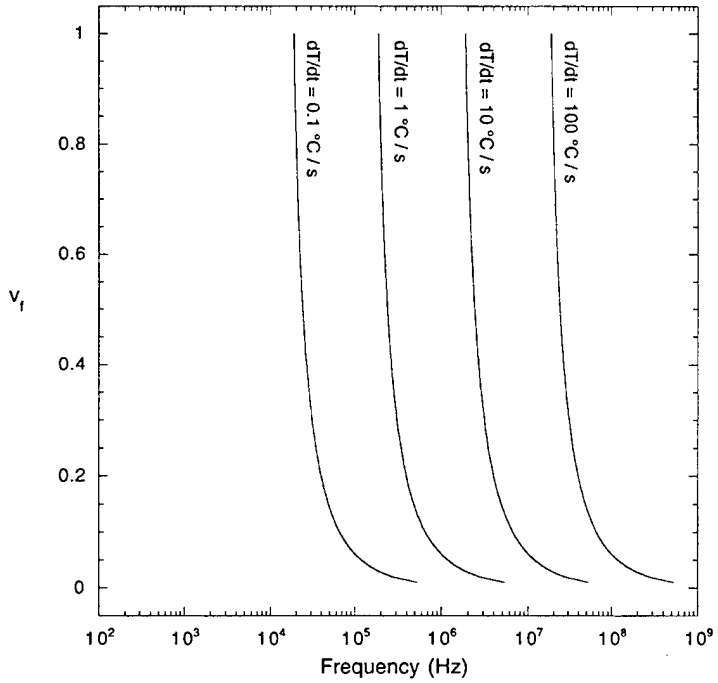

Figure 18. Strontium Ferrite Particle Volume Fraction as a Function of Frequency for Various Film Heating Rates.

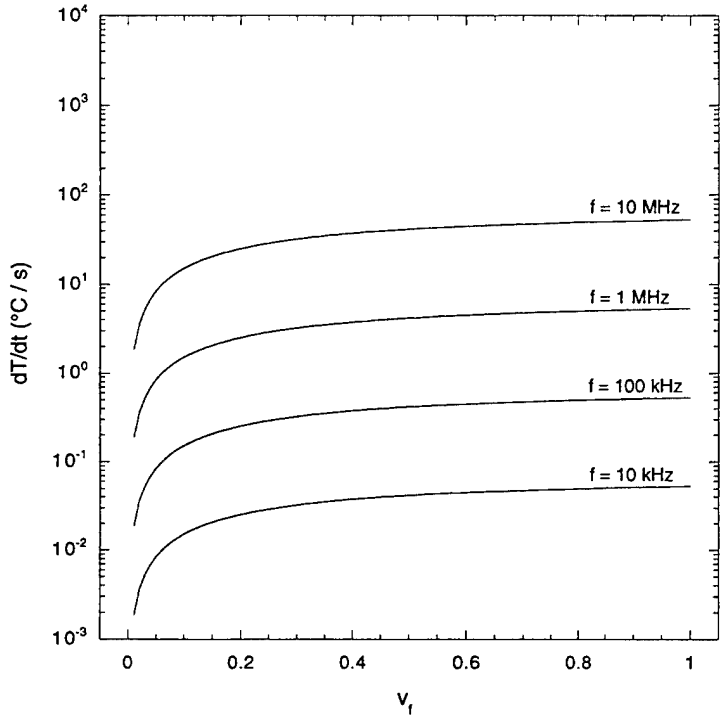

Figure 19. Heating Rates as a Function of Strontium Ferrite Particle Volume Fraction for Various Frequencies.

Table 4. NiZn Ferrite Thermophysical and Magnetic Properties. All values above horizontal line from Snelling [33]. All values below line determined graphically from Figure 21.

Property	Value
Density (ρ)	4500 kg/m^3
Specific heat (c_p)	750 J/kg K
Electrical resistivity (ρ_Ω)	10^3 Ω m
Curie temperature	100-600°C
Saturation hysteresis energy density (E_{hs})	560 J/m^3
Saturation applied field (H_s)	4.0 kA/m
Effective relative magnetic permeability ($\bar{\mu}_r$)	37.2

$\bar{\mu}_r$ value of 37.2 suggests that at our expected maximum applied field strength, 3500 A/m, the material magnetization will be $B_p = 0.16$ T.

Using equation 56 and the values of ρ_Ω and $\bar{\mu}_r$ from Table 4, the penetration thickness material parameter Υ_2 has a value for NiZn ferrite of

$$\Upsilon_2 = 5.18\ \Omega^{1/2}\mathrm{m}^{1/2}. \tag{69}$$

From Figure 8, we can see that for this value of Υ_2 shielding effects should not be important. For example, at 100 MHz, shielding should not be important if the particle diameters are less than 4 cm.

Using equation 36 and the values of E_{hs} and H_s from Table 4, we calculate $\bar{\mu}_h = 28.9$. Substituting this value with the values of ρ_Ω and $\bar{\mu}_r$ into equation 53, the heating ratio parameter Υ_1 has a value for NiZn ferrite of

$$\Upsilon_1 = 5.0 \times 10^{-2}\ \Omega^{-1}\mathrm{m}^{-1}. \tag{70}$$

This value of Υ_1 does not even appear in Figure 7. For example, at a frequency of 100 MHz, eddy heating becomes important when D_o =4 cm. Therefore Curie temperature control should not be a problem for NiZn ferrites.

Using the hysteresis energy density approximation, equation 35, with the values of E_{hs} and H_s from Table 4 and a peak applied field magnitude of $H_p = 3500$ A/m, the hysteresis power density for NiZn ferrite is 429 J/m^3. Combining this value with equation 58 and the material

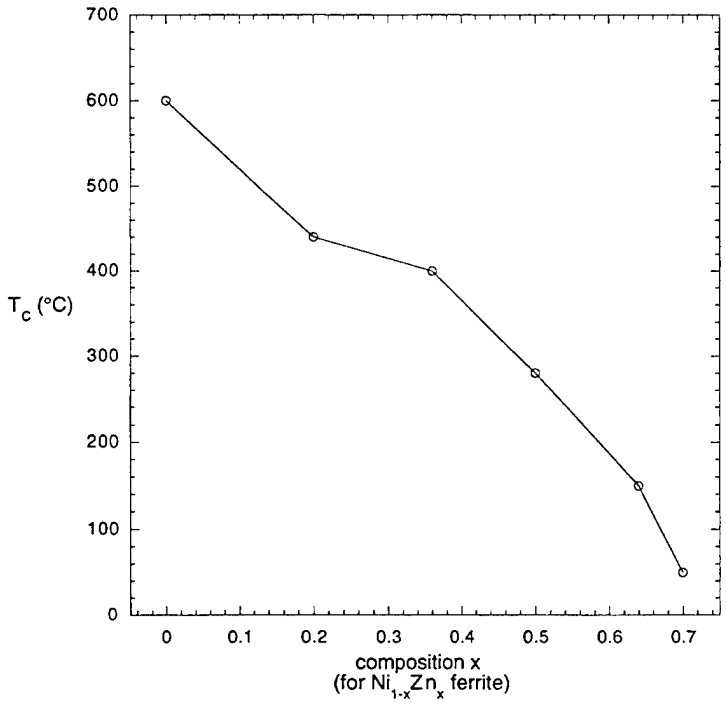

Figure 20. Curie Temperature as a Function of Composition for NiZn Ferrite (from McCurrie [32]).

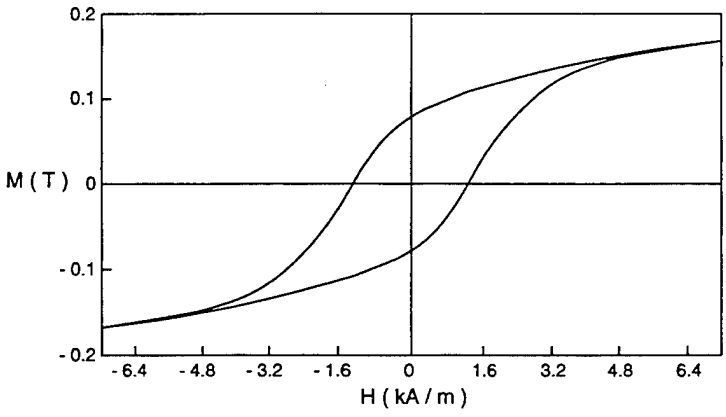

Figure 21. DC Saturation Hysteresis Curve for NiZn Ferrite (from Snelling [33]).

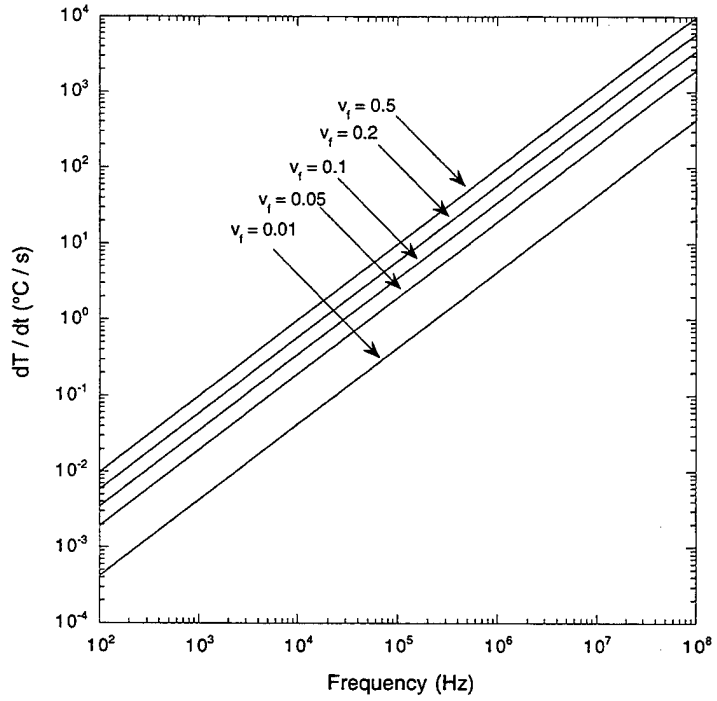

Figure 22. Heating Rate as a Function of Frequency for NiZn Ferrite Particles of Various Volume Fractions in a Polymer Film.

properties from Table 4, the heating rate for a particle / polymer film is

$$\frac{dT}{dt} \cong f(4.29 \times 10^{-4})\,(2.38 + 1/v_f)^{-1}\,. \tag{71}$$

Figure 22 shows the characteristic heating rate as a function of frequency for various volume fractions. Figure 23 shows the same information, but in terms of volume fractions for various heating rates. Figure 24 shows heating rates as a function of particle volume fraction for various frequencies. Note that reasonable heating rates are possible at frequencies of 100 kHz. These heating rates are roughly one order of magnitude greater than the heating rates calculated for nickel and strontium ferrite. At 10 MHz and $v_f = 10\%$, heating rates exceeding 100°C/s are possible.

5. Analysis

5.1 Accuracy of Models. Before making conclusions and recommendations concerning particle-based induction heating, we must discuss the accuracy of the calculations performed in this report. The eddy current model (section 2.2), given accurate material properties,

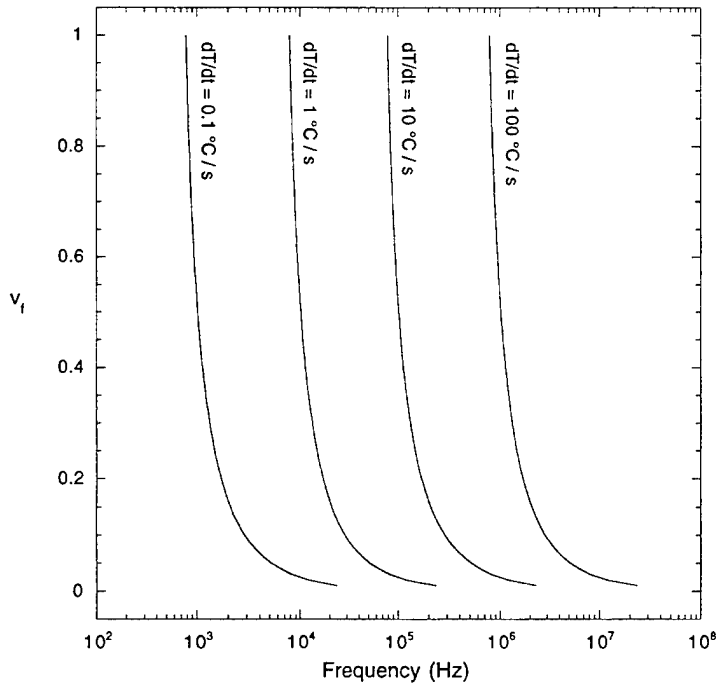

Figure 23. NiZn Ferrite Particle Volume Fraction as a Function of Frequency for Various Film Heating Rates.

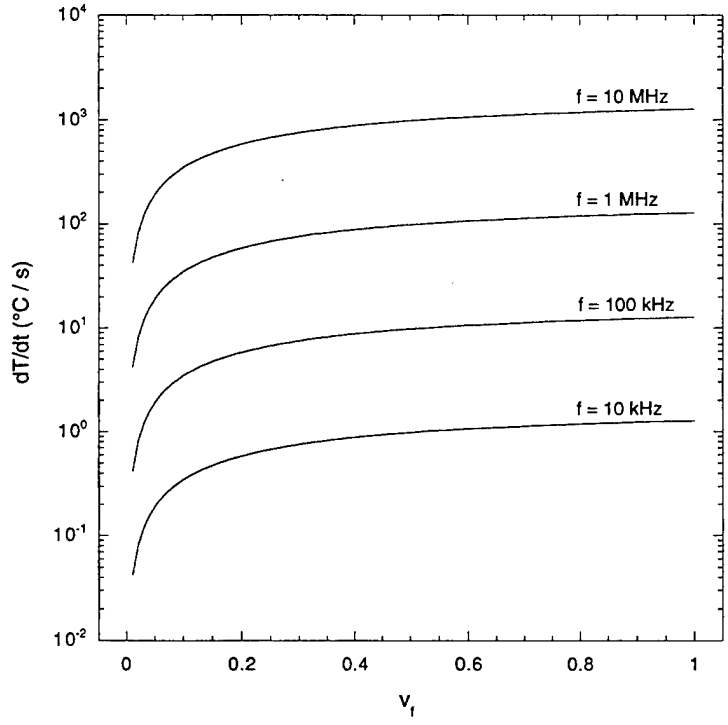

Figure 24. Heating Rates as a Function of NiZn Ferrite Particle Volume Fraction for Various Frequencies.

should be very accurate. The assumptions of uniform field and properties within the particle are certainly valid for the small particles we expect to be using. However, because we do not know the exact material permeability and resistivity at every temperature, frequency, and applied field strength, the quantitative accuracy of the results cannot be guaranteed. We can instead expect accuracy within one or two orders of magnitude.

The hysteresis heating model (section 2.3) should be very accurate, given accurate hysteresis energy density functions. For the case of NiZn ferrite, we are given a DC hysteresis curve that is within our applied field capabilities. Therefore, at low frequencies, the calculation should be extremely accurate. The hysteresis loop, however, may change dramatically as the frequency is increased, so a high level of accuracy at higher frequencies is not guaranteed. For the nickel and strontium ferrite cases, our hysteresis heating calculations are dependent on the estimation minor hysteresis loops based on a saturation hysteresis measurement. The loop self-similarity approach which we have taken is the a reasonable way to perform these calculations, but the accuracy of this approach, even within a few orders of magnitude, is not guaranteed until it is tested experimentally.

The penetration thickness model (section 2.4) should be very accurate, although we are again limited by the accuracy of the magnetic permeability values.

The induction head model (section 2.5) should be accurate for the particular geometry given. However it must be emphasized that the magnetic field strength produced by a piece of equipment is determined by the power supply specifications and the geometry of the induction coil. We have performed calculations for one typical coil and power supply, but many other options are available.

The heat transfer model (section 2.6) should be extremely accurate, and the thermophysical material properties used in the calculations are known to a high degree of accuracy. The calculations of section 4.1 also show that, as long as the particles are kept to a 1-10 μm size, the uniform heating assumption should be valid. This model however only predicts the temperature change for an insulated film. In joining applications, the film is sandwiched between two other non–heat generating composite adherends. The adherends act as heat sinks, drawing thermal energy away from the bondline. Therefore the actual heating rates produced in joining experiments will be less than those predicted by this model and measured in insulated film experiments.

In summary, the fundamental forms of all of the models are well-grounded in the physics of heat transfer and electromagnetism. The calculations are only limited by the accuracy of the material properties, especially magnetic material properties. However we should expect that all calculations are accurate to within one or two orders of magnitude, which is adequate

for this type of general strategic overview. If more quantitative modeling is to be done in the future, significant effort must be invested into collecting accurate magnetic material data.

5.2 Comparison of Materials. The calculations of section 4.2 show that nickel particles will provide adequate heating rates for joining of composite materials. For example, heating rates of 1°C/s are possible at a frequency of 1 MHz and a volume fraction of 7%. At 10 MHz, a dispersion with 7% volume fraction would heat at 10°C/s. However, size issues may become important. For example, our calculations showed that at high frequencies the particles may need to be less than 1 μm in order to prevent shielding and eddy current effects. If our material property data is inaccurate, these maximum particle sizes could be even smaller. As particle sizes approach the nanometer size range, special problems arise. These difficulties are discussed in section 5.3.

The calculations of section 4.3 show that strontium ferrite particles will provide adequate heating rates for joining of composite materials under similar conditions as nickel particles. However, unlike nickel, shielding and eddy heating effects are insignificant for any particles less than 1 cm in diameter. This difference is due to the nine orders of magnitude difference between the resistivity of nickel and strontium ferrite. The low resistivity of ferrites is therefore extremely beneficial. Even at very high frequencies, shielding and eddy heating effects will not constrain the maximum particle size, and we can avoid any potential difficulties associated with nanometer-sized particles.

The calculations of section 4.4 show that NiZn ferrite particles will provide excellent heating rates for joining of composite materials, even at moderate frequencies and low volume fractions. For example, heating rates of 50°C/s are possible at a frequency of 1 MHz and a volume fraction of 15%. NiZn ferrites also have the high resistivity common to all ferrites, so that shielding and eddy heating effects are never important.

A comparison of the important behaviors of the nickel, strontium ferrite, and NiZn ferrite materials is given in Table 5. From the table it is clear that shielding and eddy heating effects may limit the maximum frequency for processing using nickel particles, but no practical frequency limit exists for processing using ferrite particles. The comparison of hysteresis energy density E_h also shows why NiZn ferrite provides a heating rate one order of magnitude greater than nickel and strontium ferrite, since heating rate is proportional to E_h (equation 58).

This hysteresis energy density comparison is shown graphically in Figure 25 for an alternating field of maximum strength 3500 A/m. Because the applied field strength is similar to the H_s of the NiZn ferrite, its hysteresis loop is utilized fully. Nickel has a much higher H_s and lower $\bar{\mu}_r$, so it is not fully magnetized at this field strength. It is also evident that the energy

Table 5. Performance Comparison of Magnetic Materials.

Property	Nickel	Strontium ferrite	NiZn ferrite
Frequency at which D_o=1 μm particle has significant shielding	68 MHz	4.7×10^{10} GHz	2.1×10^{8} GHz
Frequency at which $D_o = 1\mu$m particle has significant eddy heating	8.5 MHz	3.3×10^{10} GHz	1.6×10^{8} GHz
E_h for H_p=3500 A/m	15.7 J/m^3	19.1 J/m^3	429 J/m^3

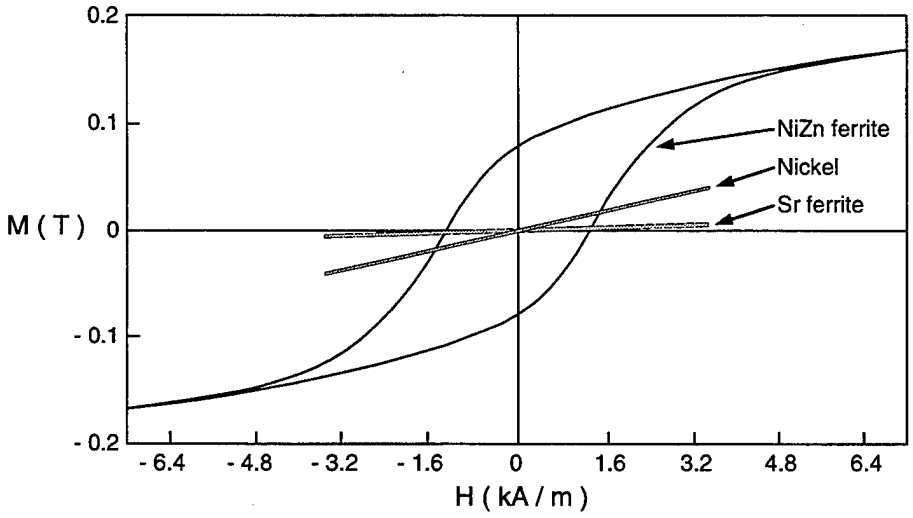

Figure 25. Comparison of Hysteresis Curves of Nickel, NiZn Ferrite, and Sr Ferrite in an AC Field with Maximum Field of 3500 A/m.

density of nickel is reduced because its hysteresis loop is not very "square" (Figure 12). Comparing the hysteresis curve for strontium ferrite in Figure 25 with its saturation hysteresis curve (Figure 16) dramatically illustrates the ineffectiveness of using hard ferrites (permanent magnet materials) for heating in low-strength fields. Hard ferrites have larger DC saturation hysteresis loop areas than soft ferrites. However, the coercivities necessary to reach saturation in these materials ($\sim 100 - 1000$ kA/m) is many orders of magnitude greater than we can ever apply with practical portable equipment, and the resulting saturation magnetization is not necessarily any greater than the saturation magnetization of soft ferrites. This statement is equivalent to the observation that hard ferrites have extremely low permeabilities. Permanent magnet materials are designed to resist changes in magnetization by an applied magnetic field. Therefore, in the presence of modest alternating magnetic fields, the resulting change in magnetization is extremely low and hysteresis heating is negligible.

The generalization that soft ferrites are superior to hard ferrites is not entirely true, however. The typical coercivity range of soft ferrites is only $\sim 1 - 100$ A/m, which is much smaller than the applied fields our equipment should be capable of. We will be able to easily saturate the material, but the total energy required to do so is not significant. The most efficient heating instead occurs if the susceptor material has a coercivity roughly equal to our maximum applied field, ~ 1000 A/m, as was the case for the particular grade of NiZn ferrite which was used for our calculations. However, this value of coercivity is unusually high for a soft ferrite. The types of materials which are best suited for our heating applications would probably be called "semi-hard" magnetic materials. Because of their moderate coercivities, they would prove inferior to other materials for most conventional hard and soft magnetic material applications. For this reason there is very little research on or commercialization of these materials.

Although the coercivity of the particular NiZn ferrite grade used in this report is nearly ideal, the saturation magnetization is actually relatively low, around 0.15 T. As a comparison, the saturation magnetization of elemental iron is over 2 T. Therefore there is a potential order of magnitude gain in the hysteresis energy density if the proper material can be found.

5.3 Size Effects. Using very small particles has a number of advantages. For a particulate film with a given volume fraction of particles, the uniformity of heat generation will be higher if the particles are smaller, since the average spacing between particles is reduced. Shielding effects and eddy current heating, phenomena which limit the applicability of our approach, are reduced as particle size is decreased. Smaller particles should provide less of a detriment to the mechanical properties of the film than large particles. This feature is especially important for composite materials, whose micrometer-sized microstructure is carefully

designed for optimum macroscopic properties. Smaller particles also should have less of an effect on the effective viscosity of the film during processing, as compared with larger particles.

However, as particle sizes approach the nanometer size range, special problems arise. In order to produce the films, the particles must be dispersed in a polymer matrix. Melt processing is the most likely approach. Nanometer-sized particles have significant inter-particle forces which may make dispersion difficult. For metal particles, oxidation is an additional problem. The extremely high surface area to mass ratio of nanometer-sized particles causes rapid, high–conversion percentage oxidation. For nickel, the resulting oxide is not magnetic or conductive, so that the heating ability of the particles is greatly reduced or even eliminated. Special environmental handling or encapsulation could be used to prevent oxidation, but would require additional research to implement.

Production of nanometer-sized particles is also difficult, particularly with metallic materials. Micrometer-sized particles can be created relatively easily using mechanical methods. In contrast, nanometer-sized particles require either extremely precise (and expensive) mechanical equipment or special techniques such as sputtering or laser ablation. These smaller particle methods also typically have much lower yields than more conventional mechanical techniques. Furthermore, alloying materials is difficult at such small size scales, because the individual constituents tend to separate.

6. Conclusions

6.1 Ideal Material and Equipment Characteristics. From our calculations and analysis, we can now state the ideal material and equipment characteristics for optimum induction heating performance and applicability. We seek a material with very high resistivity, in order to minimize shielding effects and eddy current heating. The hysteresis loop in the presence of a high frequency ($>$ 10 kHz) and moderate amplitude ($\sim$ 3500 A/m) field should have maximum area. In terms of magnetic material properties, high hysteresis losses under such conditions requires high relative magnetic permeability ($>$ 100) and coercivities in the 1-10 kA/m range. Loop "squareness" is also beneficial. We are ultimately interested in polymer processing between 100° and 400°C, and would like to be able to customize our processing temperature within $\sim$ 10°C. Rather than try to find 25 different materials, each with a Curie temperature at a different temperature, we would rather find one material or class of materials whose Curie temperature can be precisely controlled through alloying or processing history. The NiZn ferrite is an excellent example of this, with its Curie temperature very precisely determined by the relative proportions of nickel and zinc ferrite in the structure.

The size of the particles should be kept small, to avoid shielding and eddy current effects, to minimize particle influence on bulk mechanical and viscous properties, and to make heating in the film uniform. However, the particles should be kept above the nanometer size range to avoid oxidation, dispersion, and production difficulties. The 1-10 μm size range seems to offer the best compromise of these properties.

Higher frequency induction heating equipment provides higher heating rates in susceptor materials, until shielding effects begin to limit the field strength in the particle. For 1 μm diameter conductive particles, this upper frequency is around 10 MHz. For the insulating ferrites, the upper frequency is much higher. It is also possible that the hysteresis mechanisms in the particle change at very high frequencies. However, until such limiting mechanisms are identified, very high frequency field sources, including microwave sources, should be pursued.

6.2 Summary.

Some of the most important conclusions from this study are:

- Metallic particles produce reasonable heating rates but are susceptible to shielding and eddy heating effects at higher frequencies.
- Low resistivity materials, such as ferrites, are not susceptible to shielding and eddy heating effects at practical frequencies.
- Hard magnetic materials have generally too low a permeability and too high a coercivity to be useful for hysteresis heating.
- Soft magnetic materials generally have adequate permeability to be useful for hysteresis heating, but often have too low of a coercivity.
- The ideal material for hysteresis heating applications has a coercivity in a range which is not useful for most other magnetic applications. For this reason, such "semi-hard" materials have not been investigated significantly.
- With NiZn ferrite particles, excellent heating rates can be attained with available equipment (1-10 kW, 100 kHz-10 MHz) and low particle volume fractions ($\sim$ 10%).
- Keeping particle sizes in the 1-10 μm range should provide uniform film heating, eliminate shielding and eddy effects, and allow easy particle production.
- Accurate mathematical models of the relevant process physics for the particle film induction heating process can be written. However, the accuracy of their implementation

is seriously limited by the unavailability of the proper magnetic property data in the literature.

7. Recommendations for Future Work

Based on the conclusions of this report, we can recommend a number of research thrusts which will allow for the implementation and sophistication of the particle induction heating process. These research areas, which are discussed in the following sections, include:

- Preliminary induction heating experiments with NiZn ferrite particle / polymer films and adhesive pastes,
- A comprehensive literature and commercial search to find candidate materials with high potential for hysteresis heating applications,
- Design and implementation of a device for direct measurement of E_h,
- Experimentation to determine the feasibility of microwave induction processing,
- Literature search on magnetic resonance phenomenon, to determine the feasibility of improved heating through precise selection of source frequency, and
- Determination of the potential enhancement of hysteresis energy density through the use of nanometer-sized particles.

7.1 Preliminary Experiments with NiZn Ferrite. The calculations of section 4.4 show that NiZn ferrite should provide excellent heating rates in magnetic fields of 100 kHz-1 MHz, which is within the frequency range of existing equipment at the U.S. Army Research Laboratory and the University of Delaware Center for Composite Materials (CCM). NiZn ferrite is also available commercially, is inexpensive, and can be found in many grades (e. g. Steward USA, Chatanooga, TN; Ceramic Magnets, Fairfield, NJ; Fair-Rite Products, Wallkill, NY; Powder Tech, Valparaiso, IN). NiZn ferrite powder should be acquired and simple film heating tests performed. Consolidating a film / powder / film sandwich in a hot press can be used to manufacture the film. The film can be insulated and placed in a known magnetic field, and the temperature measured as a function of time.

7.2 Magnetic Materials Literature Search. Extensive literature exists on magnetic materials and their properties. A literature search needs to be performed to find general classes of materials and compositional families which have the optimal properties described in section 6.1. This search should include, but not be limited to, scientific journals, patent disclosures, and commercial databases. It will also be important to determine general effects of specific elemental additives or processing conditions on relevant magnetic properties, which permit exploration of previously untested materials.

7.3 Direct Measurement of E_h. In order to assess and optimize the heating potential of a material, its hysteresis energy density E_h needs to be measured as a function of frequency, applied field amplitude, and temperature. Equipment exists for measuring initial permeability and loss tangents as a function of frequency, and DC hysteresis loops as a function of applied field amplitude and temperature. However, all of these measurements only allow us to partially infer E_h for a given set of conditions.

A tool is needed which can directly measure E_h as a function of frequency, applied field amplitude, and temperature. The applied field strength must be variable up to 10 kA/m, and have a frequency range of 10 kHz-100 MHz. The measurements should only require a small sample mass, so that expensive or difficult to attain materials can be tested. The device should also have temperature measurement and control capabilities.

An extensive search needs to be undertaken to determine if such a device already exists. Devices which measure loss tangents are candidates, as well as transformer core loss measurement equipment.

If existing devices cannot be found that meet our requirements, new equipment needs to be designed and constructed. The device needs to generate an oscillating magnetic field in a small sample of material. The power consumed can be measured electrically, in terms of power supply power, or thermally, for example through measurement of temperature rise of a nitrogen stream flowing past the sample. The unit must also have an integrated temperature control and inert atmosphere capability. Note that in both of these scenarios, no magnetic measurements need to made. We are only measuring power consumption in a mass of material. Construction of such a device should be possible with reasonable resources.

7.4 Microwave Processing. According to our models, the heating power in the film increases proportionally with frequency. Our calculations also show that with ferrites shielding does not become important until very high frequencies. Therefore microwave frequency magnetic waves ($f > 1$ GHz) should provide extremely efficient heating. It is possible that at

such high frequencies, the hysteresis heat generation mechanisms change. Experiments will provide qualitative evidence of the feasibility of microwave heating. Candidate equipment includes standard 1 kW 2.45 GHz microwave ovens, or the 6 kW 2.45 GHz multi-mode microwave chamber at CCM. Based on our earlier calculations, NiZn ferrite particles could be used as the susceptor material.

7.5 Magnetic Resonance. All of the calculations in this report assume that the hysteresis energy density of the susceptor materials does not change with frequency. However, at very high frequencies, this assumption is not correct. The material does not have sufficient time to respond to the applied magnetic field, and so it does not fully magnetize. We expect that this effect will lower the energy density of the material as frequency increases. However, at these high frequencies, low-amplitude magnetic losses become significant. At a critical frequency the material is in a state of magnetic resonance [34], where low-amplitude losses in the material are maximized. Magnetic resonance frequencies are typically in the 100 MHz-10 GHz range. The existence of this resonant behavior implies that it may be advantageous to "tune" the applied field frequency to a specific frequency, rather than trying to maximize power through maximization of source frequency. It is not clear, however, whether magnetic resonance can produce energy densities comparable to lower frequency, high amplitude hysteresis mechanisms. A careful investigation, primarily through literature investigation, needs to be performed to determine the importance of magnetic resonance effects.

7.6 Submicron Particle Issues. The magnetic properties of materials become size-dependent as the particle size approaches the nanometer size scale. It is possible that reducing particle size to the nanometer size scale could result in significant enhancement of the hysteresis energy density of a material. E_h needs to be measured as a function of particle size to determine if this effect is significant.

Many other issues associated with nanoparticles exist, including particle production, dispersion, and oxidation prevention. However, all of these potential problems can be avoided by using micron-sized particles. In addition, this report finds no overwhelming advantages to using nanometer-sized particles. Therefore, the investigation of the production, dispersion, and oxidation of nanometer particles should not be pursued until clear benefits of nanometer particles are identified.

INTENTIONALLY LEFT BLANK.

8. References

1. Cosenza, F. "Mechanical Fasteners for Composites." *Materials Engineering*, vol. 104, no. 8, pp. 33–37, 1987.

2. Marinelli, J. M., and C. L. T. Lambing. "Study of Surface Treatments for Adhesive Bonding of Composite Materials." *Advanced Materials: Performance Through Technology Insertion International SAMPE Symposium and Exhibition (Proceedings)*, Covina, CA, vol. 38, pp. 1196–1210, 1993.

3. McKnight, S. H., B. K. Fink, S. Wells, S. Yarlagadda, and J. W. Gillespie. "Accelerated Adhesive Curing for Induction-Based Repair of Composites." ARL-TR-XX, U.S. Army Research Laboratory, Aberdeen Proving Ground, MD, to be published.

4. Holmes, S. T. "A Study of the Processing and Performance of Large-Scale Resistance Welded Thermoplastic Joints." Master's thesis, University of Delaware, Newark, DE, 1993.

5. Don, R. C., C. L. T. Lambing, and J. W. Gillespie. "Experimental Characterization of Processing-Performance Relationships of Resistance Welded Graphite / Polyetheretherketone Composite Joints." *Polym. Eng. Sci.*, vol. 32, pp. 620–631, 1992.

6. Immordino, K. M., S. H. McKnight, and J. W. Gillespie. "In-situ Evaluation of the Diffusion of Epoxy and Amine in Thermoplastic Polymers." *Journal of Adhesion*, vol. 65, pp. 115–129, 1998.

7. Wetzel, E. D., R. C. Don, and J. W. Gillespie. "Modeling Thermal Degradation during Thermoplastic Fusion Bonding of Thermoset Composites." *ANTEC Conference Proceedings*, San Francisco, CA, pp. 1263–1268, 1994.

8. Harras, B., K. C. Cole, and T. Vu-Khanh. "Characterization of Ultrasonically Welded PEEK-Carbon Composites." *Composites for Real World International SAMPE Technical Conference*, Orlando, FL, vol. 29, pp. 475–485, 1997.

9. Stokes, V. K. "Analysis of the Friction (Spin)-Welding Process for Thermoplastics." *J. Mat. Sci.*, vol. 23, pp. 2772–2785, 1988.

10. Karamuk, E., E. D. Wetzel, and J. W. Gillespie. "Modeling and Design of Induction Bonding Process for Infrastructure Rehabilitation with Composite Materials." *ANTEC Conference Proceedings*, Boston, MA, pp. 1239–1243, 1995.

11. Fink, B. K., R. L. McCullough, and J. W. Gillespie. "A Model to Predict the Through-Thickness Distribution of Heat Generation in Carbon-Fiber Composites Subjected to Alternating Magnetic Fields." *Compos. Sci. Tech.*, vol. 55, pp. 119–130, 1995.

12. Lin, W., A. K. Miller, and O. Buneman. "Predictive Capabilities of an Induction Heating Model for Complex-Shape Graphite Fiber/Polymer Matrix Composites." *International SAMPE Electronics Conference (Proceedings)*, Toronto, Ont., Can., vol. 24, pp. 606–620, 1992.

13. Fink, B. K., R. L. McCullough, and J. W. Gillespie. "A Local Theory of Heating in Cross-Ply Carbon Fiber Thermoplastic Composites by Magnetic Induction." *Polym. Eng. Sci.*, vol. 32, pp. 357–369, 1992.

14. Fink, B. K., J. Q. Xiao, J. W. Gillespie, and S. Yarlagadda. "Self-Regulating Optimized Ferromagnetic Susceptors for Multi-Step Induction Heating." Disclosure completed, 1997.

15. Magana, L. F., M. A. Escobar, and R. Valenzuela. "Effect of the Grain Size Distribution on the Ferromagnetic Hysteresis Loop." *Phys. Stat. Sol.*, vol. 97, pp. 495–500, 1986.

16. Lin, I., R. K. Mishra, and G. Thomas. "Interaction of Magnetic Domain Walls with Microstructural Features in Spinel Ferrites." *IEEE Trans. Mag.*, vol. MAG-20, pp. 134–139, 1984.

17. Escobar, M. A., and R. Valenzuela. "Analytical Prediction of the Magnetization Curve and the Ferromagnetic Hysteresis Loop." *J. Appl. Phys.*, vol. 54, pp. 5935–5940, 1983.

18. Guyot, M., and A. Globus. "Determination of the Domain Wall Energy from Hysteresis Loops in YIG." *Phys. Stat. Sol.*, vol. 59, pp. 447–454, 1973.

19. Kittel, C. "Physical Theory of Ferromagnetic Domains." *Rev. Mod. Phys.*, vol. 21, pp. 541–583, 1949.

20. Bonet, E., W. Wernsdorfer, B. Barbara, A. Benoit, D. Mailly, and A. Thiaville. "Three-Dimensional Magnetization Reversal Measurements in Nanoparticles." *Phys. Rev. Lett.*, vol. 83, pp. 4188–4191, 1999.

21. Thiaville, A. "Extensions of the Geometric Solution of the Two Dimensional Coherent Magnetization Rotation Model." *J. Magn. Magn. Mater.*, vol. 182, pp. 5–18, 1998.

22. Stoner, E. C., and E. P. Wohlfarth. "A Mechanism of Magnetic Hysteresis in Heterogeneous Alloys." *Phil. Trans. Roy. Soc. London*, vol. A240, pp. 599–642, 1948.

23. Brachtendorf, H. G., and R. Laur. "Modeling of Hysteresis in Magnetic Cores with Frequency-Dependent Losses." *J. Magn. Magn. Mater.*, vol. 183, pp. 305–312, 1998.

24. Guyot, M., T. Merceron, and V. Cagan. "Domain Wall Dynamics and Relaxation Through the Frequency Dependence of Hysteresis Loops." *J. Appl. Phys.*, vol. 57, pp. 4180–4182, 1985.

25. Cullity, B. D. *Introduction to Magnetic Materials*. Reading, MA: Addison-Wesley Publishing Company, 1972, p. 341.

26. Griffiths, D. J. *Introduction to Electrodynamics.* Englewood Cliffs, NJ: Prentice Hall, 1989.

27. Weast, R. C. *CRC Handbook of Chemistry and Physics.* Boca Raton, FL: CRC Press, 1988.

28. Suwanwatana, W. Personal communication. University of Delaware, Newark, DE, 1999.

29. Ozisik, M. N. *Heat Transfer: A Basic Approach.* New York, NY: McGraw Hill, 1985.

30. Stark, P. Personal communication. Triton Systems, Inc., Chelmsford, MA, 1999.

31. McCurrie, R. A. *Ferromagnetic Materials: Structure and Properties.* New York, NY: Academic Press, 1994, p. 244.

32. McCurrie, R. A. *Ferromagnetic Materials: Structure and Properties.* New York, NY: Academic Press, 1994, p. 149.

33. Snelling, E. C. *Soft Ferrites: Properties and Applications.* London: ILIFFE Books Ltd., 1969.

34. Gieraltowski, J., and A. Globus. "Domain Wall Size and Magnetic Losses in Frequency Spectra of Ferrites and Garnets." *IEEE Trans. Magn.*, vol. MAG-13, pp. 1357–1359, 1977.

INTENTIONALLY LEFT BLANK.

NO. OF COPIES	ORGANIZATION
2	DEFENSE TECHNICAL INFORMATION CENTER DTIC DDA 8725 JOHN J KINGMAN RD STE 0944 FT BELVOIR VA 22060-6218
1	HQDA DAMO FDT 400 ARMY PENTAGON WASHINGTON DC 20310-0460
1	OSD OUSD(A&T)/ODDDR&E(R) R J TREW THE PENTAGON WASHINGTON DC 20301-7100
1	DPTY CG FOR RDA US ARMY MATERIEL CMD AMCRDA 5001 EISENHOWER AVE ALEXANDRIA VA 22333-0001
1	INST FOR ADVNCD TCHNLGY THE UNIV OF TEXAS AT AUSTIN PO BOX 202797 AUSTIN TX 78720-2797
1	DARPA B KASPAR 3701 N FAIRFAX DR ARLINGTON VA 22203-1714
1	US MILITARY ACADEMY MATH SCI CTR OF EXCELLENCE MADN MATH MAJ HUBER THAYER HALL WEST POINT NY 10996-1786
1	DIRECTOR US ARMY RESEARCH LAB AMSRL D D R SMITH 2800 POWDER MILL RD ADELPHI MD 20783-1197

NO. OF COPIES	ORGANIZATION
1	DIRECTOR US ARMY RESEARCH LAB AMSRL DD 2800 POWDER MILL RD ADELPHI MD 20783-1197
1	DIRECTOR US ARMY RESEARCH LAB AMSRL CI AI R (RECORDS MGMT) 2800 POWDER MILL RD ADELPHI MD 20783-1145
3	DIRECTOR US ARMY RESEARCH LAB AMSRL CI LL 2800 POWDER MILL RD ADELPHI MD 20783-1145
1	DIRECTOR US ARMY RESEARCH LAB AMSRL CI AP 2800 POWDER MILL RD ADELPHI MD 20783-1197
	ABERDEEN PROVING GROUND
4	DIR USARL AMSRL CI LP (BLDG 305)

NO. OF COPIES	ORGANIZATION
1	DIRECTOR US ARMY RESEARCH LAB AMSRL CP CA D SNIDER 2800 POWDER MILL RD ADELPHI MD 20783-1145
1	DIRECTOR US ARMY RESEARCH LAB AMSRL OP SD TA 2800 POWDER MILL RD ADELPHI MD 20783-1145
3	DIRECTOR US ARMY RESEARCH LAB AMSRL OP SD TL 2800 POWDER MILL RD ADELPHI MD 20783-1145
1	DIRECTOR US ARMY RESEARCH LAB AMSRL OP SD TP 2800 POWDER MILL RD ADELPHI MD 20783-1145
1	DIRECTOR DA OASARDA SARD SO 103 ARMY PENTAGON WASHINGTON DC 20310-0103
1	DPTY ASST SECY FOR R&T SARD TT THE PENTAGON RM 3EA79 WASHINGTON DC 20301-7100
1	COMMANDER US ARMY MATERIEL CMD AMXMI INT 5001 EISENHOWER AVE ALEXANDRIA VA 22333-0001
2	COMMANDER US ARMY ARDEC AMSTA AR AE WW E BAKER J PEARSON PICATINNY ARSENAL NJ 07806-5000

NO. OF COPIES	ORGANIZATION
1	COMMANDER US ARMY ARDEC AMSTA AR TD C SPINELLI PICATINNY ARSENAL NJ 07806-5000
1	COMMANDER US ARMY ARDEC AMSTA AR FSE PICATINNY ARSENAL NJ 07806-5000
6	COMMANDER US ARMY ARDEC AMSTA AR CCH A W ANDREWS S MUSALLI R CARR M LUCIANO E LOGSDEN T LOUZEIRO PICATINNY ARSENAL NJ 07806-5000
4	COMMANDER US ARMY ARDEC AMSTA AR CC G PAYNE J GEHBAUER C BAULIEU H OPAT PICATINNY ARSENAL NJ 07806-5000
1	COMMANDER US ARMY ARDEC AMSTA AR CCH P J LUTZ PICATINNY ARSENAL NJ 07806-5000
1	COMMANDER US ARMY ARDEC AMSTA AR FSF T C LIVECCHIA PICATINNY ARSENAL NJ 07806-5000

NO. OF COPIES	ORGANIZATION
1	COMMANDER US ARMY ARDEC AMSTA AR QAC T C C PATEL PICATINNY ARSENAL NJ 07806-5000
1	COMMANDER US ARMY ARDEC AMSTA AR M D DEMELLA PICATINNY ARSENAL NJ 07806-5000
3	COMMANDER US ARMY ARDEC AMSTA AR FSA A WARNASH B MACHAK M CHIEFA PICATINNY ARSENAL NJ 07806-5000
2	COMMANDER US ARMY ARDEC AMSTA AR FSP G M SCHIKSNIS D CARLUCCI PICATINNY ARSENAL NJ 07806-5000
1	COMMANDER US ARMY ARDEC AMSTA AR FSP A P KISATSKY PICATINNY ARSENAL NJ 07806-5000
2	COMMANDER US ARMY ARDEC AMSTA AR CCH C H CHANIN S CHICO PICATINNY ARSENAL NJ 07806-5000
9	COMMANDER US ARMY ARDEC AMSTA AR CCH B P DONADIA F DONLON P VALENTI C KNUTSON G EUSTICE S PATEL G WAGNECZ R SAYER F CHANG PICATINNY ARSENAL NJ 07806-5000
6	COMMANDER US ARMY ARDEC AMSTA AR CCL F PUZYCKI R MCHUGH D CONWAY E JAROSZEWSKI R SCHLENNER M CLUNE PICATINNY ARSENAL NJ 07806-5000
1	COMMANDER US ARMY ARDEC AMSTA AR QAC T D RIGOGLIOSO PICATINNY ARSENAL NJ 07806-5000
1	COMMANDER US ARMY ARDEC AMSTA AR SRE D YEE PICATINNY ARSENAL NJ 07806-5000
1	COMMANDER US ARMY ARDEC AMSTA AR WET T SACHAR BLDG 172 PICATINNY ARSENAL NJ 07806-5000

NO. OF COPIES	ORGANIZATION
1	COMMANDER US ARMY ARDEC AMSTA ASF PICATINNY ARSENAL NJ 07806-5000
1	US ARMY ARDEC INTELLIGENCE SPECIALIST AMSTA AR WEL F M GUERRIERE PICATINNY ARSENAL NJ 07806-5000
11	PM TMAS SFAE GSSC TMA R MORRIS C KIMKER D GUZOWICZ E KOPACZ R ROESER R DARCY R MCDANOLDS L D ULISSE C ROLLER J MCGREEN B PATTER PICATINNY ARSENAL NJ 07806-5000
2	PEO FIELD ARTILLERY SYS SFAE FAS PM H GOLDMAN T MCWILLIAMS PICATINNY ARSENAL NJ 07806-5000
1	COMMANDER US ARMY TACOM PM ABRAMS SFAE ASM AB 6501 ELEVEN MILE RD WARREN MI 48397-5000
6	PM SADARM SFAE GCSS SD COL B ELLIS M DEVINE R KOWALSKI W DEMASSI J PRITCHARD S HROWNAK PICATINNY ARSENAL NJ 07806-5000
1	COMMANDER US ARMY ARDEC PRODUCTION BASE MODERN ACTY AMSMC PBM K PICATINNY ARSENAL NJ 07806-5000
3	COMMANDER US ARMY TACOM PM TACTICAL VEHICLES SFAE TVL SFAE TVM SFAE TVH 6501 ELEVEN MILE RD WARREN MI 48397-5000
1	COMMANDER US ARMY TACOM PM BFVS SFAE ASM BV 6501 ELEVEN MILE RD WARREN MI 48397-5000
1	COMMANDER US ARMY TACOM PM AFAS SFAE ASM AF 6501 ELEVEN MILE RD WARREN MI 48397-5000
1	COMMANDER US ARMY TACOM PM RDT&E SFAE GCSS W AB J GODELL 6501 ELEVEN MILE RD WARREN MI 48397-5000

NO. OF COPIES	ORGANIZATION
2	COMMANDER US ARMY TACOM PM SURV SYS SFAE ASM SS T DEAN SFAE GCSS W GSI M D COCHRAN 6501 ELEVEN MILE RD WARREN MI 48397-5000
1	COMMANDER US ARMY TACOM PM SURVIVABLE SYSTEMS SFAE GCSS W GSI H M RYZYI 6501 ELEVEN MILE RD WARREN MI 48397-5000
1	COMMANDER US ARMY TACOM PM BFV SFAE GCSS W BV S DAVIS 6501 ELEVEN MILE RD WARREN MI 48397-5000
1	COMMANDER US ARMY TACOM PM LIGHT TACTICAL VHCLS AMSTA TR S A J MILLS MS 209 6501 ELEVEN MILE RD WARREN MI 48397-5000
1	COMMANDER US ARMY TACOM PM GROUND SYSTEMS INTEGRATION SFAE GCSS W GSI R LABATILLE 6501 ELEVEN MILE RD WARREN MI 48397-5000
1	COMMANDER US ARMY TACOM CHIEF ABRAMS TESTING SFAE GCSS W AB QT T KRASKIEWICZ 6501 ELEVEN MILE RD WARREN MI 48397-5000

NO. OF COPIES	ORGANIZATION
14	COMMANDER US ARMY TACOM AMSTA TR R J CHAPIN R MCCLELLAND D THOMAS J BENNETT D HANSEN AMSTA JSK S GOODMAN J FLORENCE K IYER J THOMSON AMSTA TR D D OSTBERG L HINOJOSA B RAJU AMSTA CS SF H HUTCHINSON F SCHWARZ WARREN MI 48397-5000
1	COMMANDER US ARMY TACOM AMSTA SF WARREN MI 48397-5000
1	COMMANDER WATERVLIET ARSENAL SMCWV QAE Q B VANINA BLDG 44 WATERVLIET NY 12189-4050
1	COMMANDER WATERVLIET ARSENAL SMCWV SPM T MCCLOSKEY BLDG 253 WATERVLIET NY 12189-4050
2	TSM ABRAMS ATZK TS S JABURG W MEINSHAUSEN FT KNOX KY 40121

NO. OF COPIES	ORGANIZATION
10	BENET LABORATORIES AMSTA AR CCB R FISCELLA G D ANDREA M SCAVULO G SPENCER P WHEELER K MINER J VASILAKIS G FRIAR R HASENBEIN AMSTA CCB R S SOPOK WATERVLIET NY 12189-4050
3	ARMOR SCHOOL ATZK TD R BAUEN J BERG A POMEY FT KNOX KY 40121
2	HQ IOC TANK AMMUNITION TEAM AMSIO SMT R CRAWFORD W HARRIS ROCK ISLAND IL 61299-6000
1	DIRECTOR US ARMY AMCOM SFAE AV RAM TV D CALDWELL BLDG 5300 REDSTONE ARSENAL AL 35898
2	COMMANDER US ARMY AMCOM AVIATION APPLIED TECH DIR J SCHUCK FT EUSTIS VA 23604-5577
1	US ARMY CERL R LAMPO 2902 NEWMARK DR CHAMPAIGN IL 61822

NO. OF COPIES	ORGANIZATION
4	DIRECTOR US ARMY CECOM NIGHT VISION & ELECTRONIC SENSORS DIR AMSEL RD NV CM CCD R ADAMS R MCLEAN A YINGST AMSEL RD NV VISP E JACOBS 10221 BURBECK RD FT BELVOIR VA 22060-5806
2	US ARMY CORPS OF ENGINEERS CERD C T LIU CEW ET T TAN 20 MASS AVE NW WASHINGTON DC 20314
1	US ARMY COLD REGIONS RSCH & ENGRNG LAB P DUTTA 72 LYME RD HANOVER NH 03755
1	SYSTEM MANAGER ABRAMS ATZK TS LTC J H NUNN BLDG 1002 RM 110 FT KNOX KY 40121
1	CHIEF USAIC ATZB COM LTC T J CUMMINGS FT BENNING GA 31905-5800
1	USA SBCCOM PM SOLDIER SPT AMSSB PM RSS A J CONNORS KANSAS ST NATICK MA 01760-5057

NO. OF COPIES	ORGANIZATION
8	DIRECTOR US ARMY NATIONAL GROUND INTELLIGENCE CTR D LEITER M HOLTUS M WOLFE S MINGLEDORF J GASTON W GSTATTENBAUER R WARNER J CRIDER 220 SEVENTH ST NE CHARLOTTESVILLE VA 22091
6	US ARMY SBCCOM SOLDIER SYSTEMS CENTER BALLISTICS TEAM J WARD MARINE CORPS TEAM J MACKIEWICZ BUS AREA ADVOCACY TEAM W HASKELL SSCNC WST W NYKVIST T MERRILL S BEAUDOIN KANSAS ST NATICK MA 01760-5019
9	US ARMY RESEARCH OFC A CROWSON J CHANDRA H EVERETT J PRATER R SINGLETON G ANDERSON D STEPP D KISEROW J CHANG PO BOX 12211 RESEARCH TRIANGLE PARK NC 27709-2211
1	NAVAL SURFACE WARFARE CTR DAHLGREN DIV CODE G06 DAHLGREN VA 22448

NO. OF COPIES	ORGANIZATION
1	NAVAL SURFACE WARFARE CTR TECH LIBRARY CODE 323 17320 DAHLGREN RD DAHLGREN VA 22448
3	NAVAL RESEARCH LAB I WOLOCK CODE 6383 R BADALIANCE CODE 6304 L GAUSE WASHINGTON DC 20375
1	NAVAL SURFACE WARFARE CTR CRANE DIVISION M JOHNSON CODE 20H4 LOUISVILLE KY 40214-5245
2	COMMANDER NAVAL SURFACE WARFARE CTR CARDEROCK DIVISION R PETERSON CODE 2020 M CRITCHFIELD CODE 1730 BETHESDA MD 20084
2	NAVAL SURFACE WARFARE CTR U SORATHIA C WILLIAMS CD 6551 9500 MACARTHUR BLVD WEST BETHESDA MD 20817
1	DAVID TAYLOR RESEARCH CTR SHIP STRUCTURES & PROTECTION DEPT CODE 1702 BETHESDA MD 20084
2	DAVID TAYLOR RESEARCH CTR R ROCKWELL W PHYILLAIER BETHESDA MD 20054-5000
1	OFC OF NAVAL RESEARCH D SIEGEL CODE 351 800 N QUINCY ST ARLINGTON VA 22217-5660

NO. OF COPIES	ORGANIZATION
8	NAVAL SURFACE WARFARE CTR J FRANCIS CODE G30 D WILSON CODE G32 R D COOPER CODE G32 J FRAYSSE CODE G33 E ROWE CODE G33 T DURAN CODE G33 L DE SIMONE CODE G33 R HUBBARD CODE G33 DAHLGREN VA 22448
1	NAVAL SEA SYSTEMS CMD D LIESE 2531 JEFFERSON DAVIS HWY ARLINGTON VA 22242-5160
1	NAVAL SURFACE WARFARE CTR M LACY CODE B02 17320 DAHLGREN RD DAHLGREN VA 22448
1	OFC OF NAVAL RES J KELLY 800 NORTH QUINCEY ST ARLINGTON VA 22217-5000
2	NAVAL SURFACE WARFARE CTR CARDEROCK DIVISION R CRANE CODE 2802 C WILLIAMS CODE 6553 3A LEGGETT CIR BETHESDA MD 20054-5000
1	EXPEDITIONARY WARFARE DIV N85 F SHOUP 2000 NAVY PENTAGON WASHINGTON DC 20350-2000
1	AFRL MLBC 2941 P ST RM 136 WRIGHT PATTERSON AFB OH 45433-7750
1	AFRL MLSS R THOMSON 2179 12TH ST RM 122 WRIGHT PATTERSON AFB OH 45433-7718

NO. OF COPIES	ORGANIZATION
2	AFRL F ABRAMS J BROWN BLDG 653 2977 P ST STE 6 WRIGHT PATTERSON AFB OH 45433-7739
1	AFRL MLS OL L COULTER 7278 4TH ST BLDG 100 BAY D HILL AFB UT 84056-5205
1	OSD JOINT CCD TEST FORCE OSD JCCD R WILLIAMS 3909 HALLS FERRY RD VICKSBURG MS 29180-6199
1	DEFENSE NUCLEAR AGENCY INNOVATIVE CONCEPTS DIV 6801 TELEGRAPH RD ALEXANDRIA VA 22310-3398
1	WATERWAYS EXPERIMENT D SCOTT 3909 HALLS FERRY RD SC C VICKSBURG MS 39180
3	DARPA M VANFOSSEN S WAX L CHRISTODOULOU 3701 N FAIRFAX DR ARLINGTON VA 22203-1714
2	FAA TECH CENTER D OPLINGER AAR 431 P SHYPRYKEVICH AAR 431 ATLANTIC CITY NJ 08405
2	SERDP PROGRAM OFC PM P2 C PELLERIN B SMITH 901 N STUART ST STE 303 ARLINGTON VA 22203

NO. OF COPIES	ORGANIZATION
1	FAA MIL HDBK 17 CHAIR L ILCEWICZ 1601 LIND AVE SW ANM 115N RESTON VA 98055
1	US DEPT OF ENERGY OFC OF ENVIRONMENTAL MANAGEMENT P RITZCOVAN 19901 GERMANTOWN RD GERMANTOWN MD 20874-1928
1	DIRECTOR LLNL F ADDESSIO MS B216 PO BOX 1633 LOS ALAMOS NM 87545
5	DIRECTOR LLNL R CHRISTENSEN S DETERESA F MAGNESS M FINGER MS 313 M MURPHY L 282 PO BOX 808 LIVERMORE CA 94550
1	OAK RIDGE NATIONAL LABORATORY R M DAVIS PO BOX 2008 OAK RIDGE TN 37831-6195
1	OAK RIDGE NATIONAL LABORATORY C EBERLE MS 8048 PO BOX 2009 OAK RIDGE TN 37831
1	OAK RIDGE NATIONAL LABORATORY C D WARREN MS 8039 PO BOX 2009 OAK RIDGE TN 37922

NO. OF COPIES	ORGANIZATION
7	NIST R PARNAS J DUNKERS M VANLANDINGHAM MS 8621 J CHIN MS 8621 D HUNSTON MS 8543 J MARTIN MS 8621 D DUTHINH MS 8611 100 BUREAU DR GAITHERSBURG MD 20899
1	HYDROGEOLOGIC INC SERDP ESTCP SPT OFC S WALSH 1155 HERNDON PKWY STE 900 HERNDON VA 20170
3	DIRECTOR SANDIA NATIONAL LABS APPLIED MECHANICS DEPT DIV 8241 J HANDROCK Y R KAN J LAUFFER PO BOX 969 LIVERMORE CA 94550-0096
3	NASA LANGLEY RSCH CTR AMSRL VS W ELBER MS 266 F BARTLETT JR MS 266 G FARLEY MS 266 HAMPTON VA 23681-0001
1	NASA LANGLEY RSCH CTR T GATES MS 188E HAMPTON VA 23661-3400
1	USDOT FEDERAL RAILRD M FATEH RDV 31 WASHINGTON DC 20590
1	FHWA E MUNLEY 6300 GEORGETOWN PIKE MCLEAN VA 22101

NO. OF COPIES	ORGANIZATION
1	CENTRAL INTLLGNC AGNCY OTI WDAG GT W L WALTMAN PO BOX 1925 WASHINGTON DC 20505
1	MARINE CORPS INTLLGNC ACTVTY D KOSITZKE 3300 RUSSELL RD STE 250 QUANTICO VA 22134-5011
1	DIRECTOR NATIONAL GRND INTLLGNC CTR IANG TMT 220 SEVENTH ST NE CHARLOTTESVILLE VA 22902-5396
1	DIRECTOR DEFENSE INTLLGNC AGNCY TA 5 K CRELLING WASHINGTON DC 20310
1	GRAPHITE MASTERS INC J WILLIS 3815 MEDFORD ST LOS ANGELES CA 90063-1900
1	ADVANCED GLASS FIBER YARNS T COLLINS 281 SPRING RUN LANE STE A DOWNINGTON PA 19335
1	COMPOSITE MATERIALS INC D SHORTT 19105 63 AVE NE PO BOX 25 ARLINGTON WA 98223
1	COMPOSITE MATERIALS INC R HOLLAND 11 JEWEL CT ORINDA CA 94563
1	COMPOSITE MATERIALS INC C RILEY 14530 S ANSON AVE SANTA FE SPRINGS CA 90670

NO. OF COPIES	ORGANIZATION
2	COMPOSIX D BLAKE L DIXON 120 O NEILL DR HEBRUN OHIO 43025
4	CYTEC FIBERITE R DUNNE D KOHLI M GILLIO R MAYHEW 1300 REVOLUTION ST HAVRE DE GRACE MD 21078
2	SIMULA J COLTMAN R HUYETT 10016 S 51ST ST PHOENIX AZ 85044
1	SIOUX MFG B KRIEL PO BOX 400 FT TOTTEN ND 58335
2	PROTECTION MATERIALS INC M MILLER F CRILLEY 14000 NW 58 CT MIAMI LAKES FL 33014
3	FOSTER MILLER J J GASSNER M ROYLANCE W ZUKAS 195 BEAR HILL RD WALTHAM MA 02354-1196
1	ROM DEVELOPMENT CORP R O MEARA 136 SWINEBURNE ROW BRICK MARKET PLACE NEWPORT RI 02840
2	TEXTRON SYSTEMS T FOLTZ M TREASURE 201 LOWELL ST WILMINGTON MA 08870-2941

NO. OF COPIES	ORGANIZATION
1	JPS GLASS L CARTER PO BOX 260 SLATER RD SLATER SC 29683
1	O GARA HESS & EISENHARDT M GILLESPIE 9113 LESAINT DR FAIRFIELD OH 45014
2	MILLIKEN RSCH CORP H KUHN M MACLEOD PO BOX 1926 SPARTANBURG SC 29303
1	CONNEAUGHT INDUSTRIES INC J SANTOS PO BOX 1425 COVENTRY RI 02816
2	BATTELLE NATICK OPNS J CONNORS B HALPIN 209 W CENTRAL ST STE 302 NATICK MA 01760
1	ARMTEC DEFENSE PRODUCTS S DYER 85 901 AVE 53 PO BOX 848 COACHELLA CA 92236
1	GLCC INC J RAY 103 TRADE ZONE DR STE 26C WEST COLUMBIA SC 29170
3	PACIFIC NORTHWEST LAB M SMITH G VAN ARSDALE R SHIPPELL PO BOX 999 RICHLAND WA 99352

NO. OF COPIES	ORGANIZATION
2	AMOCO PERFORMANCE PRODUCTS M MICHNO JR J BANISAUKAS 4500 MCGINNIS FERRY RD ALPHARETTA GA 30202-3944
1	SAIC M PALMER 1410 SPRING HILL RD STE 400 MS SH4 5 MCLEAN VA 22102
1	SAIC G CHRYSSOMALLIS 3800 W 80TH ST STE 1090 BLOOMINGTON MN 55431
1	AAI CORPORATION T G STASTNY PO BOX 126 HUNT VALLEY MD 21030-0126
1	APPLIED COMPOSITES W GRISCH 333 NORTH SIXTH ST ST CHARLES IL 60174
3	ALLIANT TECHSYSTEMS INC J CONDON E LYNAM J GERHARD WV01 16 STATE RT 956 PO BOX 210 ROCKET CENTER WV 26726-0210
1	CUSTOM ANALYTICAL ENG SYS INC A ALEXANDER 13000 TENSOR LANE NE FLINTSTONE MD 21530
1	OFC DEPUTY UNDER SEC DEFNS JAMES THOMPSON 1745 JEFFERSON DAVIS HWY CRYSTAL SQ 4 STE 501 ARLINGTON VA 22202

NO. OF COPIES	ORGANIZATION
8	ALLIANT TECHSYSTEMS INC C CANDLAND MN11 2830 C AAKHUS MN11 2830 B SEE MN11 2439 N VLAHAKUS MN11 2145 R DOHRN MN11 2830 S HAGLUND MN11 2439 M HISSONG MN11 2830 D KAMDAR MN11 2830 600 SECOND ST NE HOPKINS MN 55343-8367
1	PROJECTILE TECHNOLOGY INC 515 GILES ST HAVRE DE GRACE MD 21078
1	LORAL VOUGHT SYSTEMS K COOK 1701 W MARSHALL DR GRAND PRAIRIE TX 75051
5	AEROJET GEN CORP D PILLASCH T COULTER C FLYNN D RUBAREZUL M GREINER 1100 WEST HOLLYVALE ST AZUSA CA 91702-0296
3	HEXCEL INC R BOE F POLICELLI J POESCH PO BOX 98 MAGNA UT 84044
1	HERCULES INC HERCULES PLAZA WILMINGTON DE 19894
1	BRIGS COMPANY J BACKOFEN 2668 PETERBOROUGH ST HERNDON VA 22071-2443
1	ZERNOW TECHNICAL SERVICES L ZERNOW 425 W BONITA AVE STE 208 SAN DIMAS CA 91773
2	OLIN CORPORATION FLINCHBAUGH DIV E STEINER B STEWART PO BOX 127 RED LION PA 17356
1	OLIN CORPORATION L WHITMORE 10101 NINTH ST NORTH ST PETERSBURG FL 33702
1	GKN AEROSPACE D OLDS 15 STERLING DR WALLINGFORD CT 06492
5	SIKORSKY AIRCRAFT G JACARUSO T CARSTENSAN B KAY S GARBO MS S330A J ADELMANN 6900 MAIN ST PO BOX 9729 STRATFORD CT 06497-9729
1	PRATT & WHITNEY C WATSON 400 MAIN ST MS 114 37 EAST HARTFORD CT 06108
1	AEROSPACE CORP G HAWKINS M4 945 2350 E EL SEGUNDO BLVD EL SEGUNDO CA 90245
2	CYTEC FIBERITE M LIN W WEB 1440 N KRAEMER BLVD ANAHEIM CA 92806

NO. OF COPIES	ORGANIZATION
1	HEXCEL T BITZER 11711 DUBLIN BLVD DUBLIN CA 94568
1	BOEING R BOHLMANN PO BOX 516 MC 5021322 ST LOUIS MO 63166-0516
2	BOEING DFNSE & SPACE GP W HAMMOND S 4X55 J RUSSELL S 4X55 PO BOX 3707 SEATTLE WA 98124-2207
2	BOEING ROTORCRAFT P MINGURT P HANDEL 800 B PUTNAM BLVD WALLINGFORD PA 19086
1	BOEING DOUGLAS PRODUCTS DIV L J HART SMITH 3855 LAKEWOOD BLVD D800 0019 LONG BEACH CA 90846-0001
1	LOCKHEED MARTIN S REEVE 8650 COBB DR D 73 62 MZ 0648 MARIETTA GA 30063-0648
1	LOCKHEED MARTIN SKUNK WORKS D FORTNEY 1011 LOCKHEED WAY PALMDALE CA 93599-2502
1	LOCKHEED MARTIN R FIELDS 1195 IRWIN CT WINTER SPRINGS FL 32708
1	MATERIALS SCIENCES CORP B W ROSEN 500 OFC CENTER DR STE 250 FT WASHINGTON PA 19034
1	NORTHRUP GRUMMAN CORP ELECTRONIC SENSORS & SYSTEMS DIV E SCHOCH MS V 16 1745A W NURSERY RD LINTHICUM MD 21090
2	NORTHROP GRUMMAN ENVIRONMENTAL PROGRAMS R OSTERMAN A YEN 8900 E WASHINGTON BLVD PICO RIVERA CA 90660
1	UDLP D MARTIN PO BOX 359 SANTA CLARA CA 95052
1	UDLP G THOMAS PO BOX 58123 SANTA CLARA CA 95052
2	UDLP R BARRETT MAIL DROP M53 V HORVATICH MAIL DROP M53 328 W BROKAW RD SANTA CLARA CA 95052-0359
3	UDLP GROUND SYSTEMS DIVISION M PEDRAZZI MAIL DROP N09 A LEE MAIL DROP N11 M MACLEAN MAIL DROP N06 1205 COLEMAN AVE SANTA CLARA CA 95052
4	UDLP R BRYNSVOLD P JANKE MS 170 4800 EAST RIVER RD MINNEAPOLIS MN 55421-1498
1	GDLS DIVISION D BARTLE PO BOX 1901 WARREN MI 48090

NO. OF COPIES	ORGANIZATION
2	GDLS D REES M PASIK PO BOX 2074 WARREN MI 48090-2074
1	GDLS MUSKEGON OPERATIONS W SOMMERS JR 76 GETTY ST MUSKEGON MI 49442
1	GENERAL DYNAMICS AMPHIBIOUS SYS SURVIVABILITY LEAD G WALKER 991 ANNAPOLIS WAY WOODBRIDGE VA 22191
5	INST FOR ADVANCED TECH T KIEHNE H FAIR P SULLIVAN W REINECKE I MCNAB 4030 2 W BRAKER LN AUSTIN TX 78759
2	CIVIL ENGR RSCH FOUNDATION PRESIDENT H BERNSTEIN R BELLE 1015 15TH ST NW STE 600 WASHINGTON DC 20005
1	ARROW TECH ASSO 1233 SHELBURNE RD STE D 8 SOUTH BURLINGTON VT 05403-7700
1	R EICHELBERGER CONSULTANT 409 W CATHERINE ST BEL AIR MD 21014-3613
1	UCLA MANE DEPT ENGR IV H T HAHN LOS ANGELES CA 90024-1597

NO. OF COPIES	ORGANIZATION
2	UNIV OF DAYTON RESEARCH INST R Y KIM A K ROY 300 COLLEGE PARK AVE DAYTON OH 45469-0168
1	MIT P LAGACE 77 MASS AVE CAMBRIDGE MA 01887
1	IIT RESEARCH CENTER D ROSE 201 MILL ST ROME NY 13440-6916
1	GA TECH RSCH INST GA INST OF TCHNLGY P FRIEDERICH ATLANTA GA 30392
1	MICHIGAN ST UNIV MSM DEPT R AVERILL 3515 EB EAST LANSING MI 48824-1226
1	UNIV OF KENTUCKY L PENN 763 ANDERSON HALL LEXINGTON KY 40506-0046
1	UNIV OF WYOMING D ADAMS PO BOX 3295 LARAMIE WY 82071
1	UNIV OF UTAH DEPT OF MECH & INDUSTRIAL ENGR S SWANSON SALT LAKE CITY UT 84112
2	PENN STATE UNIV R MCNITT C BAKIS 212 EARTH ENGR SCIENCES BLDG UNIVERSITY PARK PA 16802

NO. OF COPIES	ORGANIZATION
1	PENN STATE UNIV R S ENGEL 245 HAMMOND BLDG UNIVERSITY PARK PA 16801
1	PURDUE UNIV SCHOOL OF AERO & ASTRO C T SUN W LAFAYETTE IN 47907-1282
1	STANFORD UNIV DEPT OF AERONAUTICS & AEROBALLISTICS S TSAI DURANT BLDG STANFORD CA 94305
1	UNIV OF DAYTON J M WHITNEY COLLEGE PARK AVE DAYTON OH 45469-0240
7	UNIV OF DELAWARE CTR FOR COMPOSITE MTRLS J GILLESPIE M SANTARE G PALMESE S YARLAGADDA S ADVANI D HEIDER D KUKICH 201 SPENCER LABORATORY NEWARK DE 19716
1	DEPT. OF MATERIALS SCIENCE & ENGINEERING UNIVERSITY OF ILLINOIS AT URBANA CHAMPAIGN J ECONOMY 1304 WEST GREEN ST URBANA IL 61801
1	NORTH CAROLINA STATE UNIV CIVIL ENGINEERING DEPT W RASDORF PO BOX 7908 RALEIGH NC 27696-7908

NO. OF COPIES	ORGANIZATION
3	THE UNIV OF TEXAS AT AUSTIN CTR FOR ELECTROMECHANICS J PRICE A WALLS J KITZMILLER 10100 BURNET RD AUSTIN TX 78758-4497
3	VA POLYTECHNICAL INST & STATE UNIV DEPT OF ESM M W HYER K REIFSNIDER R JONES BLACKSBURG VA 24061-0219
1	UNIV OF MARYLAND DEPT OF AEROSPACE ENGNRNG A J VIZZINI COLLEGE PARK MD 20742
1	DREXEL UNIV A S D WANG 32ND & CHESTNUT ST PHILADELPHIA PA 19104
1	SOUTHWEST RSCH INST ENGR & MATL SCIENCES DIV J RIEGEL 6220 CULEBRA RD PO DRAWER 28510 SAN ANTONIO TX 78228-0510
	ABERDEEN PROVING GROUND
1	US ARMY MATERIEL SYSTEMS ANALYSIS P DIETZ 392 HOPKINS RD AMXSY TD APG MD 21005-5071
1	DIRECTOR US ARMY RESEARCH LAB AMSRL OP AP L APG MD 21005-5066

NO. OF COPIES	ORGANIZATION
	ABERDEEN PROVING GROUND (CONT)
106	DIR USARL
	AMSRL CI
	AMSRL CI H
	W STUREK
	AMSRL CI S
	A MARK
	AMSRL CS IO FI
	M ADAMSON
	AMSRL SL B
	J SMITH
	AMSRL SL BA
	AMSRL SL BL
	D BELY
	R HENRY
	AMSRL SL BG
	AMSRL SL I
	AMSRL WM B
	A HORST
	E SCHMIDT
	AMSRL WM BA
	F BRANDON
	AMSRL WM BC
	P PLOSTINS
	D LYON
	J NEWILL
	S WILKERSON
	A ZIELINSKI
	AMSRL WM BD
	B FORCH
	R FIFER
	R PESCE RODRIGUEZ
	B RICE
	AMSRL WM BE
	C LEVERITT
	D KOOKER
	AMSRL WM BR
	C SHOEMAKER
	J BORNSTEIN
	AMSRL WM M
	D VIECHNICKI
	G HAGNAUER
	J MCCAULEY
	B TANNER
	AMSRL WM MA
	R SHUFORD
	P TOUCHET
	N BECK TAN

NO. OF COPIES	ORGANIZATION
	ABERDEEN PROVING GROUND (CONT)
	AMSRL WM MA
	D FLANAGAN
	L GHIORSE
	D HARRIS
	S MCKNIGHT
	P MOY
	P PATTERSON
	G RODRIGUEZ
	A TEETS
	R YIN
	AMSRL WM MB
	B FINK
	J BENDER
	T BLANAS
	T BOGETTI
	R BOSSOLI
	L BURTON
	K BOYD
	S CORNELISON
	P DEHMER
	R DOOLEY
	W DRYSDALE
	G GAZONAS
	S GHIORSE
	D GRANVILLE
	D HOPKINS
	C HOPPEL
	D HENRY
	R KASTE
	M KLUSEWITZ
	M LEADORE
	R LIEB
	E RIGAS
	J SANDS
	D SPAGNUOLO
	W SPURGEON
	J TZENG
	E WETZEL
	AMSRL WM MB ALC
	A FRYDMAN
	AMRSL WM MC
	J BEATTY
	E CHIN
	J MONTGOMERY
	A WERECZCAK
	J LASALVIA
	J WELLS

NO. OF
COPIES ORGANIZATION

ABERDEEN PROVING GROUND (CONT)

AMSRL WM MD
W ROY
S WALSH
AMSRL WM T
B BURNS
AMSRL WM TA
W GILLICH
T HAVEL
J RUNYEON
M BURKINS
E HORWATH
B GOOCH
W BRUCHEY
AMSRL WM TC
R COATES
AMSRL WM TD
A DAS GUPTA
T HADUCH
T MOYNIHAN
F GREGORY
A RAJENDRAN
M RAFTENBERG
M BOTELER
T WEERASOORIYA
D DANDEKAR
A DIETRICH
AMSRL WM TE
A NIILER
J POWELL
AMSRL SS SD
H WALLACE
AMSRL SS SE R
R CHASE
AMSRL SS SE DS
R REYZER
R ATKINSON
AMSRL SE L
R WEINRAUB
J DESMOND
D WOODBURY

NO. OF COPIES	ORGANIZATION
1	LTD R MARTIN MERL TAMWORTH RD HERTFORD SG13 7DG UK
1	SMC SCOTLAND P W LAY DERA ROSYTH ROSYTH ROYAL DOCKYARD DUNFERMLINE FIFE KY 11 2XR UK
1	CIVIL AVIATION ADMINSTRATION T GOTTESMAN PO BOX 8 BEN GURION INTERNL AIRPORT LOD 70150 ISRAEL
1	AEROSPATIALE S ANDRE A BTE CC RTE MD132 316 ROUTE DE BAYONNE TOULOUSE 31060 FRANCE
3	DRA FORT HALSTEAD P N JONES M HINTON SEVEN OAKS KENT TN 147BP UK
1	DEFENSE RESEARCH ESTAB VALCARTIER F LESAGE COURCELETTE QUEBEC COA IRO CANADA
2	ROYAL MILITARY COLLEGE OF SCIENCE SHRIVENHAM D BULMAN B LAWTON SWINDON WILTS SN6 8LA UK

NO. OF COPIES	ORGANIZATION
1	SWISS FEDERAL ARMAMENTS WKS W LANZ ALLMENDSTRASSE 86 3602 THUN SWITZERLAND
1	ISRAEL INST OF TECHNOLOGY S BODNER FACULTY OF MECHANICAL ENGR HAIFA 3200 ISRAEL
1	DSTO MATERIALS RESEARCH LAB NAVAL PLATFORM VULNERABILITY SHIP STRUCTURES & MTRLS DIV N BURMAN PO BOX 50 ASCOT VALE VICTORIA AUSTRALIA 3032
1	ECOLE ROYAL MILITAIRE E CELENS AVE DE LA RENAISSANCE 30 1040 BRUXELLE BELGIQUE
1	DEF RES ESTABLISHMENT VALCARTIER A DUPUIS 2459 BOULEVARD PIE XI NORTH VALCARTIER QUEBEC CANADA PO BOX 8800 COURCELETTE GOA IRO QUEBEC CANADA
1	INSTITUT FRANCO ALLEMAND DE RECHERCHES DE SAINT LOUIS DE M GIRAUD 5 RUE DU GENERAL CASSAGNOU BOITE POSTALE 34 F 68301 SAINT LOUIS CEDEX FRANCE
1	ECOLE POLYTECH J MANSON DMX LTC CH 1015 LAUSANNE SWITZERLAND

NO. OF COPIES	ORGANIZATION
1	TNO PRINS MAURITS LABORATORY R IJSSELSTEIN LANGE KLEIWEG 137 PO BOX 45 2280 AA RIJSWIJK THE NETHERLANDS
2	FOA NATL DEFENSE RESEARCH ESTAB DIR DEPT OF WEAPONS & PROTECTION B JANZON R HOLMLIN S 172 90 STOCKHOLM SWEDEN
2	DEFENSE TECH & PROC AGENCY GROUND I CREWTHER GENERAL HERZOG HAUS 3602 THUN SWITZERLAND
1	MINISTRY OF DEFENCE RAFAEL ARMAMENT DEVELOPMENT AUTH M MAYSELESS PO BOX 2250 HAIFA 31021 ISRAEL
1	DYNAMEC RESEARCH AB AKE PERSSON BOX 201 SE 151 23 SODERTALJE SWEDEN
1	TNO DEFENSE RESEARCH I H PASMAN POSTBUS 6006 2600 JA DELFT THE NETHERLANDS
1	B HIRSCH TACHKEMONY ST 6 NETAMUA 42611 ISRAEL

NO. OF COPIES	ORGANIZATION
1	DEUTSCHE AEROSPACE AG DYNAMICS SYSTEMS M HELD PO BOX 1340 D 86523 SCHROBENHAUSEN GERMANY

INTENTIONALLY LEFT BLANK.

REPORT DOCUMENTATION PAGE

Form Approved
OMB No. 0704-0188

1. AGENCY USE ONLY *(Leave blank)*	2. REPORT DATE	3. REPORT TYPE AND DATES COVERED
	March 2001	Final, Jun 99–Aug 99

4. TITLE AND SUBTITLE
Feasibility of Magnetic Particle Films for Curie Temperature-Controlled Processing of Composite Materials

5. FUNDING NUMBERS
AH42

6. AUTHOR(S)
Eric D. Wetzel and Bruce K. Fink

7. PERFORMING ORGANIZATION NAME(S) AND ADDRESS(ES)
U.S. Army Research Laboratory
ATTN: AMSRL-WM-MB
Aberdeen Proving Ground, MD 21005-5069

8. PERFORMING ORGANIZATION REPORT NUMBER
ARL-TR-2431

9. SPONSORING/MONITORING AGENCY NAMES(S) AND ADDRESS(ES)

10.SPONSORING/MONITORING AGENCY REPORT NUMBER

11. SUPPLEMENTARY NOTES

12a. DISTRIBUTION/AVAILABILITY STATEMENT
Approved for public release; distribution is unlimited.

12b. DISTRIBUTION CODE

13. ABSTRACT*(Maximum 200 words)*

The feasibility of using magnetic particulate susceptor materials for induction heating during bonding of polymer matrix composite materials is investigated. If properly designed, these systems should rapidly heat to the particulate material Curie temperature and dwell at that temperature without feedback control. This performance is only possible by maximizing hysteresis heating while eliminating eddy current heating and shielding effects. Models of eddy current heating, hysteresis heating, field penetration thickness, and heat transfer in a particulate film are presented. These models are then used to predict heating behavior of particulate films containing metallic ferromagnetic (nickel), hard magnetic (strontium ferrite), and soft magnetic (nickel zinc ferrite) materials. The results show that soft or semi-hard insulating magnetic materials are best suited for susceptor particles for a broad range of potential military applications. Polymer films with around 10% volume fraction of these materials should be capable of heating rates up to 100 °C/s in moderate strength 1–10 MHz induction fields.

14. SUBJECT TERMS
composite material, magnetic particle, curie temperature, ferrite, nanoparticle, magnetic resonance, repair

15. NUMBER OF PAGES
76

16. PRICE CODE

17. SECURITY CLASSIFICATION OF REPORT	18. SECURITY CLASSIFICATION OF THIS PAGE	19. SECURITY CLASSIFICATION OF ABSTRACT	20. LIMITATION OF ABSTRACT
UNCLASSIFIED	UNCLASSIFIED	UNCLASSIFIED	UL

INTENTIONALLY LEFT BLANK.

USER EVALUATION SHEET/CHANGE OF ADDRESS

This Laboratory undertakes a continuing effort to improve the quality of the reports it publishes. Your comments/answers to the items/questions below will aid us in our efforts.

1. ARL Report Number/Author ARL-TR-2431 (Wetzel) Date of Report March 2001

2. Date Report Received _____

3. Does this report satisfy a need? (Comment on purpose, related project, or other area of interest for which the report will be used.) _____

4. Specifically, how is the report being used? (Information source, design data, procedure, source of ideas, etc.) _____

5. Has the information in this report led to any quantitative savings as far as man-hours or dollars saved, operating costs avoided, or efficiencies achieved, etc? If so, please elaborate. _____

6. General Comments. What do you think should be changed to improve future reports? (Indicate changes to organization, technical content, format, etc.) _____

CURRENT ADDRESS

_____
Organization

_____
Name E-mail Name

_____
Street or P.O. Box No.

_____
City, State, Zip Code

7. If indicating a Change of Address or Address Correction, please provide the Current or Correct address above and the Old or Incorrect address below.

OLD ADDRESS

_____
Organization

_____
Name

_____
Street or P.O. Box No.

_____
City, State, Zip Code

(Remove this sheet, fold as indicated, tape closed, and mail.)

(DO NOT STAPLE)